

Multi-fidelity Learning of Reduced Order Models for Parabolic PDE Constrained Optimization

Benedikt Klein ^{1*} and Mario Ohlberger ²

^{1,2}Mathematics Münster, University of Münster, Einsteinstrasse 62,
Münster, 48149, Germany.

*Corresponding author(s). E-mail(s): benedikt.klein@uni-muenster.de;
Contributing authors: mario.ohlberger@uni-muenster.de;

Abstract

This article builds on the recently proposed RB-ML-ROM approach for parameterized parabolic PDEs and proposes a novel hierarchical Trust Region algorithm for solving parabolic PDE constrained optimization problems. Instead of using a traditional offline/online splitting approach for model order reduction, we adopt an active learning or enrichment strategy to construct a multi-fidelity hierarchy of reduced order models on-the-fly during the outer optimization loop. The multi-fidelity surrogate model consists of a full order model, a reduced order model and a machine learning model. The proposed hierarchical framework adaptively updates its hierarchy when querying parameters, utilizing a rigorous a posteriori error estimator in an error aware trust region framework. Numerical experiments are given to demonstrate the efficiency of the proposed approach.

Keywords: Reduced order models, multi-fidelity learning, parabolic PDE constrained optimization, trust region algorithm

MSC Classification: 49M20 , 49K20 , 35J20 , 65N30 , 90C06

1 Introduction

Optimization problems governed by Partial Differential Equations (PDEs) play a crucial role in various fields, including physics, engineering, and economics, as they enable the modeling, solution and optimization of complex systems that involve spatially distributed phenomena. The ability to efficiently solve such optimization problems has far-reaching implications for applications like optimal control, inverse

problems, and design optimization. Typical algorithms require numerous evaluations of the underlying PDE for various parameters that are selected in an outer descent-type optimization loop. In this contribution we are concerned with a novel multi-fidelity learning approach to speed up such algorithms for parameter optimization or optimal control problems with parabolic PDE constraints. The approach builds on a hierarchy of approximate models with increasing accuracy and decreasing efficiency, consisting of a machine learning surrogate, a reduced basis model and a full order finite element model. Such an approach has recently been proposed as a certified “on demand” RB-ML-ROM learning approach to approximate parametrized input-output maps [1]. In order to efficiently handle optimization problems, we integrated this approach into the error aware trust region framework [2] that has recently been advanced theoretically and numerically in [3–5]. We now give a more detailed overview to the various techniques involved in our multi-fidelity approach.

Model order reduction for PDE constrained optimization. Model Order Reduction (MOR) methods have gained significant attention in recent years for efficiently solving parameterized PDEs [6, 7]. These methods aim to reduce the computational complexity by replacing high-dimensional Full Order Models (FOMs) with low-dimensional surrogates.

A promising approach is the usage of Reduced Basis (RB) methods, which rely on approximating the solution manifold of parameterized PDEs (pPDEs) by low-dimensional linear approximation spaces. We particularly refer to the POD-Greedy method [8, 9] as well as the Hierarchical approximate POD (HaPOD) [10] for parameterized parabolic PDEs. There is a large amount of literature using such reduced models for PDE constrained optimization, cf. [11–13]. For an introduction to MOR methods for optimal control problems we refer, e.g., to [14]. More recently, RB methods have been advised with a progressive construction of Reduced Order Models (ROMs) [15–17] which has led to a series of works on error aware trust region reduced basis methods.

Error aware Trust-Region – Reduced Basis methods. Trust-Region (TR) approaches are a class of optimization methods that build on the iterative solution of appropriately chosen locally accurate surrogate models. The main idea is to solve optimization sub-problems only in a local area of the parameter domain which resolves the burden of constructing a global RB space. TR optimization methods have been successfully combined with MOR to leverage locally accurate surrogate models, ensuring global convergence while reducing the computational cost [2, 18]. Significant further development and analysis of such approaches were presented in [3–5, 19]. We also refer to a related approach with application to shape optimization problems [20].

Data based surrogate modeling and machine learning approaches. In parallel to model-based reduction methods, purely data-based approaches for machine learning of surrogate models have increasingly been developed and mathematically investigated [21–25]. Our methodology exploits the strengths of both model-based

and data-driven approaches, enabling the construction of certified, adaptive, and efficient surrogate models. The general idea of a full order, reduced order and machine learning model pipeline has first been introduced in [26] and subsequently been put in a certified RB-ML-ROM framework in [1]. Despite deep neural networks, also kernel methods and novel deep kernel approaches have been investigated and compared [27]. For further learning based approaches for related optimization problems we refer to [28–31]. We also note that these approaches are complementary to unsupervised learning approaches, such as physics-informed neural networks [32] or, e.g., deep Ritz methods [33].

Main results. This work demonstrates the potential of combining the above mentioned approaches to tackle parameter optimization with parabolic PDE constraints or corresponding optimal control problems. We thereby integrate certified and adaptive model order reduction with machine learning techniques in a trust region optimization framework. By doing so in a multi-fidelity fashion, we overcome the limitations of traditional global model reduction methods and purely machine learning based approaches that typically come without error certification. Particular novelties of this contribution include

- a posteriori error estimates for the approximate objective function and its derivatives,
- a concept for trust region multi-fidelity optimization,
- the integration of the RB-ML-ROM surrogate modeling approach with the error aware TR optimization method,
- an efficient implementation of the resulting multi-fidelity TR-RB-ML-Opt approach based on the model reduction software framework pyMOR [34],
- a numerical proof of concept that demonstrate that our new TR-RB-ML-Opt method outperforms existing model reduction approaches.

Organization of the article. In Section 2 we introduce the parabolic PDE constrained optimization problem and discuss the adjoint problem resulting from the optimality conditions. A suitable reduced basis approximation and corresponding a posteriori error estimates are discussed in Section 3. Section 4 then introduces machine learning surrogates and adaptations that are necessary with respect to a posteriori error estimation. Finally, the trust region multi-fidelity optimization framework is introduced in Section 5. Numerical experiments in Section 6 demonstrate the performance of the resulting approach in comparison to previous TR-RB approaches.

2 Problem Formulation

Let $T > 0$ be a fixed end-time and $\Omega \subset \mathbb{R}^d$ a bounded domain with a Lipschitz continuous boundary $\partial\Omega$. We define the Hilbert spaces \mathbb{D} and V , equipped with inner products $\langle \cdot, \cdot \rangle_{\mathbb{D}}$ and $\langle \cdot, \cdot \rangle_V$, along with their induced norms $\|\cdot\|_{\mathbb{D}} := \sqrt{\langle \cdot, \cdot \rangle_{\mathbb{D}}}$ and $\|\cdot\|_V := \sqrt{\langle \cdot, \cdot \rangle_V}$. These spaces satisfy the embedding hierarchy $H_0^1(\Omega) \subset V \subset H^1(\Omega) \subset L^2(\Omega) \subset V'$.

Additionally, let $\mathcal{P} \subset \mathbb{R}^P$ be a simple bounded parameter domain, defined as $\mathcal{P} := \{x \in \mathbb{R}^P \mid L_j \leq x_j \leq U_j, \quad j = 1, \dots, P\}$, where $-\infty < L_j < U_j < \infty$. Our goal

is to determine a parameter $\mu \in \mathcal{P}$ that minimizes the time-discretized least-squares objective functional relative to a desired state $g_{\text{ref}} \in L^2(0, T; \mathbb{D})$:

$$J(u(\mu); \mu) := \Delta t \sum_{k=1}^K \|F(u^k(\mu)) - g_{\text{ref}}^k\|_{\mathbb{D}}^2 + \lambda \mathcal{R}(\mu),$$

where $g_{\text{ref}}^k := g_{\text{ref}}(t^k)$ are evaluations of g_{ref} at a uniform temporal grid $\mathcal{G}_{\Delta t}^{\text{pr}} := \{0 = t^0 < \dots < t^K = T\}$ with time step $\Delta t := t^{i+1} - t^i$. The state trajectory $u(\mu) := (u^k(\mu))_{k \in \{0, \dots, K\}}$ satisfies the time-discretized parabolic PDE:

$$\frac{1}{\Delta t} (u^k(\mu) - u^{k-1}(\mu), v)_{L^2(\Omega)} + a(u^k(\mu), v; \mu) = b(t^k) f(v; \mu), \quad u^0(\mu) = 0, \quad (1)$$

for all $k \in \mathbb{K} := \{1, \dots, K\}$ and $v \in V$. Here, for each $\mu \in \mathcal{P}$, the operator $f(\cdot; \mu) : V \rightarrow \mathbb{R}$ is a V -continuous, twice continuously differentiable linear functional with derivatives $\partial_{\mu_i} f(\cdot; \mu) \in V'$ for $i \in \{1, \dots, P\}$. The bilinear form $a(\cdot, \cdot; \mu) : V \times V \rightarrow \mathbb{R}$ is V -continuous, coercive, symmetric, and twice continuously differentiable in μ , with derivatives $a_{\mu_i} := \partial_{\mu_i} a(\cdot, \cdot; \mu)$. The mapping $F : V \rightarrow \mathbb{D}$ computes a quantity of interest for states in V , while $b : [0, T] \rightarrow \mathbb{R}$ represents a time-dependent forcing term. Regularization is ensured by a twice continuously differentiable function $\mathcal{R} : \mathcal{P} \rightarrow \mathbb{R}$ with weight $\lambda \in \mathbb{R}_{\geq 0}$. Henceforth, (1) will be referred to as the *primal problem*.

For the construction of an a posteriori error estimator, we define the inner product on V using the a -energy product at a fixed $\bar{\mu} \in \mathcal{P}$, i.e., $\langle \cdot, \cdot \rangle_V := a(\cdot, \cdot; \bar{\mu})$. We assume that for any given $\mu \in \mathcal{P}$, the coercivity and continuity constants

$$\begin{aligned} 0 < \gamma_a(\mu) &:= \sup_{w \in V \setminus \{0\}} \sup_{v \in V \setminus \{0\}} \frac{a(w, v; \mu)}{\|w\|_V \|v\|_V} < \infty, \\ 0 < \gamma_{a_{\mu_i}}(\mu) &:= \sup_{w \in V \setminus \{0\}} \sup_{v \in V \setminus \{0\}} \frac{a_{\mu_i}(w, v; \mu)}{\|w\|_V \|v\|_V} < \infty \text{ and} \\ 0 < \alpha_0^a \leq \alpha(\mu) &:= \inf_{v \in V \setminus \{0\}} \frac{a(v, v; \mu)}{\|v\|_V^2}, \end{aligned}$$

can be bounded from below, respectively from above. I.e. we assume that $\alpha_{\text{LB}}(\mu)$ and $\gamma_{a_{\mu_i}}^{\text{UB}}(\mu)$ exist such that

$$0 < \alpha_0^a \leq \alpha_{\text{LB}}(\mu) \leq \alpha(\mu) \text{ and } \gamma_{a_{\mu_i}}^{\text{UB}}(\mu) \geq \gamma_{a_{\mu_i}}(\mu).$$

Furthermore, we assume that a and f are *affinely decomposable*, meaning that

$$a(w, v; \mu) = \sum_{q=1}^{Q_a} \Theta_a^q(\mu) a^q(w, v), \quad f(v; \mu) = \sum_{\tilde{q}=1}^{Q_f} \Theta_f^{\tilde{q}}(\mu) f^{\tilde{q}}(v),$$

where the functions $\Theta_a^q, \Theta_f^{\bar{q}} : \mathcal{P} \rightarrow \mathbb{R}$ are twice continuously differentiable, while $a^q : V \times V \rightarrow \mathbb{R}$ and $f^{\bar{q}} : V \rightarrow \mathbb{R}$ are parameter-independent continuous (bi)linear forms. For notational convenience, we introduce:

$$d(w, v) := (F(w), F(v))_{\mathbb{D}}, \quad l^k(v) := -2(F(v), g_{\text{ref}}^k)_{\mathbb{D}} \text{ for } v, w \in V,$$

with continuity constants γ_d and γ_l . Throughout this work, the state trajectory $u(\mu)$ belongs to the Bochner-type Hilbert space

$$Q_{\Delta t}^{\text{pr}}(0, T; V) := \left\{ f : \mathcal{G}_{\Delta t}^{\text{pr}} \rightarrow V \mid f(t^0) = 0, \quad \|f\|_{Q_{\Delta t}^{\text{pr}}(0, T; V)} < \infty \right\}, \quad (2)$$

with inner product

$$\langle f, g \rangle_{Q_{\Delta t}^{\text{pr}}(0, T; V)} := \sum_{k=1}^K \langle f(t^k), g(t^k) \rangle_V,$$

and corresponding norm $\|\cdot\|_{Q_{\Delta t}^{\text{pr}}(0, T; V)}$. The optimization problem of interest is therefore:

Problem 2.1. Consider the minimization problem

$$\begin{aligned} & \underset{\mu \in \mathcal{P}}{\text{argmin}} \mathcal{J}(\mu), \\ \mathcal{J}(\mu) & := J(u(\mu); \mu) = \Delta t \sum_{k=1}^K [d(u^k(\mu), u^k(\mu)) + l^k(u^k(\mu)) + (g_{\text{ref}}^k, g_{\text{ref}}^k)_{\mathbb{D}}] + \lambda \mathcal{R}(\mu), \end{aligned}$$

where $u(\mu) \in Q_{\Delta t}^{\text{pr}}(0, T, V)$ satisfies (1).

Remark 2.2. Following the assumptions made above, for all $\mu \in \mathcal{P}$, a unique solution to (1) exists. Thus, the primal solution operator $A^{\text{pr}} : \mathcal{P} \rightarrow Q_{\Delta t}^{\text{pr}}(0, T; V); \mu \mapsto u(\mu)$ is well-defined. Moreover, it can be shown, cf. [35], that A^{pr} and thus $\mathcal{J}(\mu)$ are continuously differentiable with respect to μ . The i -th partial derivative will be denoted by $d_{\mu_i} \mathcal{J}(\mu)$. Furthermore, the Fréchet derivative is denoted by $\partial_{\mu} \mathcal{J}(\mu) : \mathcal{P} \rightarrow \mathbb{R}$. Note that $d_{\mu_i} \mathcal{J}(\mu) = \partial_{\mu} \mathcal{J}(\mu) \cdot e_i$, where e_i is the i -th canonical unit vector.

2.1 The Adjoint Problem

To solve optimization problem 2.1 using a gradient descent type method, efficient computation of the derivatives $d_{\mu_i} \mathcal{J}(\mu)$ is required. This can be achieved by an adjoint approach as outlined in [3, 19, 35]. For a fixed $\mu \in \mathcal{P}$, let $u(\mu) \in Q_{\Delta t}^{\text{pr}}(0, T; V)$ be the solution to (1). The *adjoint trajectory* associated to $u(\mu)$, denoted $p(\mu) := (p^k(\mu))_{k \in \{1, \dots, K+1\}}$, is given as the unique solution of

$$\begin{aligned} \frac{1}{\Delta t} (v, p^k(\mu) - p^{k+1}(\mu))_{L^2(\Omega)} + a(v, p^k(\mu); \mu) &= 2d(u^k(\mu), v) + l^k(v), \\ p^{K+1}(\mu) &= 0, \end{aligned} \quad (3)$$

for all $k \in \mathbb{K}$ and $v \in V$. The Bochner-type Hilbert space $Q_{\Delta t}^{\text{ad}}(0, T; V)$ is defined analogously to (2),

$$Q_{\Delta t}^{\text{ad}}(0, T; V) := \left\{ f : \mathcal{G}_{\Delta t}^{\text{ad}} \rightarrow V \mid f(t^{K+1}) = 0, \quad \|f\|_{Q_{\Delta t}^{\text{ad}}(0, T; V)} < \infty \right\},$$

with $\mathcal{G}_{\Delta t}^{\text{ad}} := \{\Delta t =: t^1 < \dots < t^{K+1} := T + \Delta t\}$. Following [19, 35], the first-order derivative $d_{\mu_i} \mathcal{J}(\mu)$ for $i \in \{1, \dots, P\}$ can be computed as

$$d_{\mu_i} \mathcal{J}(\mu) = \Delta t \sum_{k=1}^K [b(t^k) f_{\mu_i}(p^k(\mu); \mu) - a_{\mu_i}(u^k(\mu), p^k(\mu); \mu)] + \lambda d_{\mu_i} \mathcal{R}(\mu). \quad (4)$$

This adjoint-based approach provides computational efficiency by solving (3) instead of evaluating each derivative separately.

Remark 2.3. The formulation (4) is equivalent to $d_{\mu_i} \mathcal{J}(\mu) = d_{\mu_i} \mathcal{L}(u(\mu), \mu, p(\mu))$ (cf. [3]), where \mathcal{L} is the Lagrangian for Problem 2.1, given by

$$\begin{aligned} \mathcal{L}(u(\mu), \mu, p(\mu)) &= \mathcal{J}(\mu) + \sum_{k=1}^K b(t^k) f(p^k(\mu); \mu) - a(u^k(\mu), p^k(\mu); \mu) \\ &\quad - \frac{1}{\Delta t} (u^k(\mu) - u^{k-1}(\mu), p^k(\mu))_{L^2(\Omega)}. \end{aligned}$$

For solving (1) and its adjoint problem (3), a conventional Finite Element (FE) discretization approach is used. Consider a finite-dimensional Hilbert space $V_h \subset V$, equipped with the inner product $\langle \cdot, \cdot \rangle_V$. By projecting the primal (1) and adjoint problems (3) into V_h (Galerkin projection), we obtain well-defined approximations $u_h(\mu) \in Q_{\Delta t}^{\text{pr}}(0, T; V_h)$ and $p_h(\mu) \in Q_{\Delta t}^{\text{ad}}(0, T; V_h)$ for the exact solutions $u(\mu)$ and $p(\mu)$. The corresponding objective functional and gradient are given by

$$\mathcal{J}_h(\mu) := J(u_h(\mu); \mu), \quad d_{\mu_i} \mathcal{J}_h(\mu) = d_{\mu_i} \mathcal{L}(u_h(\mu), \mu, p_h(\mu)). \quad (5)$$

We refer to the computational model that determines, for a given parameter $\mu \in \mathcal{P}$, the high-fidelity objective functional $\mathcal{J}_h(\mu)$ and its gradient $\nabla_{\mu} \mathcal{J}_h(\mu) := (\partial_{\mu_1} \mathcal{J}_h(\mu), \dots, \partial_{\mu_P} \mathcal{J}_h(\mu))$ as the Full Order Model (FOM).

3 Reduced basis method

Ensuring satisfactory accuracy of the FOMs typically requires a high dimension of V_h , making their evaluation computationally expensive. This is especially challenging in optimization, due to the high number of parameter queries required. To mitigate the computational burdens of high-fidelity simulations, RB methods have gained considerable interest and demonstrated substantial reductions in computation time [3, 19, 36]. The properties of RB models make them also genuinely compatible with the trust-region method as will be discussed in detail in Section 5. Moreover, can RB methods act

as vital cornerstone for integrating machine learning-based surrogates in optimization problems, as a feasible option, as we will see in Section 4.

In RB methods, the high-dimensional space V_h is replaced by a subspace $V_{\text{RB}} \subset V_h$, with a significantly lower dimension and the problems (1) and (3) are solved, after projecting them into this space, allowing for faster evaluations due to the reduced dimension. Suppose a V_h -orthonormal basis $\{\psi_i, i = 1, \dots, N_{\text{RB}}\}$ is given. This *reduced basis*, define the reduced state space

$$V_{\text{RB}} := \text{span}\{\psi_i, i = 1, \dots, N_{\text{RB}}\} \subset V_h. \quad (6)$$

The RB approximation $u_{\text{RB}}(\mu) \in Q_{\Delta t}^{\text{pr}}(0, T; V_{\text{RB}})$ to the primal high-fidelity trajectory $u_h(\mu)$ thus satisfies for all $k \in \mathbb{K}$ and $v \in V_{\text{RB}}$

$$\frac{1}{\Delta t} (u_{\text{RB}}^k(\mu) - u_{\text{RB}}^{k-1}(\mu), v)_{L^2(\Omega)} + a(u_{\text{RB}}^k(\mu), v; \mu) = b(t^k) f(v; \mu), \quad u_{\text{RB}}^0(\mu) = 0. \quad (7)$$

Similarly, the approximation of the adjoint solution $p_{\text{RB}}(\mu) \in Q_{\Delta t}^{\text{ad}}(0, T; V_{\text{RB}})$ associated to $u_{\text{RB}}(\mu)$ will be obtained by solving

$$\begin{aligned} \frac{1}{\Delta t} (v, p_{\text{RB}}^k(\mu) - p_{\text{RB}}^{k+1}(\mu))_{L^2(\Omega)} + a(v, p_{\text{RB}}^k(\mu); \mu) &= 2d(u_{\text{RB}}^k(\mu), v) + l^k(v), \\ p_{\text{RB}}^{K+1}(\mu) &= 0, \end{aligned} \quad (8)$$

for all $k \in \mathbb{K}$ and $v \in V_{\text{RB}}$. The RB objective functional follows naturally from these definitions.

Definition 3.1. Let $\mu \in \mathcal{P}$ and V_{RB} as defined in (6) be given. The *RB approximate objective functional and gradient* are defined as

$$\mathcal{J}_{\text{RB}}(\mu) := J(u_{\text{RB}}(\mu); \mu) \text{ and } d_{\mu_i} \mathcal{J}_{\text{RB}}(\mu) = d_{\mu_i} \mathcal{L}(u_{\text{RB}}(\mu), \mu, p_{\text{RB}}(\mu)),$$

where $u_{\text{RB}}(\mu) \in Q_{\Delta t}^{\text{pr}}(0, T; V_{\text{RB}})$ is the solution of (7) and $p_{\text{RB}}(\mu) \in Q_{\Delta t}^{\text{ad}}(0, T; V_{\text{RB}})$ of (8), associated to $u_{\text{RB}}(\mu)$. The model returning these approximations will be referred to as *reduced basis-reduced order model (RB-ROM)*.

3.1 A Posteriori Error Estimator

For TR methods, RB approximations come with online-efficient a posteriori error estimators for the approximation error $|\mathcal{J}_h(\mu) - \mathcal{J}_{\text{RB}}(\mu)|$ and its gradient. A model is considered *certified* if such an error estimator exists. We summarize key aspects of RB error estimation here; for further details, see [19, 37, 38]. We begin by defining the residual operators for the reduced linear problems (7) and (8).

Definition 3.2 (Residual Operators). For $k \in \mathbb{K}$, define the residual operator as

$$r_{\text{pr}}^k : Q_{\Delta t}^{\text{pr}}(0, T; V_h) \times V_h \times \mathcal{P} \rightarrow \mathbb{R},$$

$$(u, v; \mu) \mapsto r_{\text{pr}}^k(u, v; \mu) := b(t^k)f(v; \mu) - a(u^k, v; \mu) - \frac{1}{\Delta t}(u^k - u^{k-1}, v)_{L^2(\Omega)}$$

for the primal case and

$$r_{\text{ad}}^k : Q_{\Delta t}^{\text{pr}}(0, T; V_h) \times Q_{\Delta t}^{\text{ad}}(0, T; V_h) \times V_h \times \mathcal{P} \rightarrow \mathbb{R},$$

$$(u, p, v; \mu) \mapsto r_{\text{ad}}^k(u, p, v; \mu) := 2d(u^k, v) + l^k(v) - a(v, p^k; \mu) - \frac{1}{\Delta t}(v, p^k - p^{k+1})_{L^2(\Omega)}$$

for the adjoint case. Define

$$r_{\text{pr}}(u, v; \mu) := (r_{\text{pr}}^k(u, v; \mu))_{k \in \mathbb{K}} \in \mathbb{R}^K,$$

$$r_{\text{ad}}(u, p, v; \mu) := (r_{\text{ad}}^k(u, p, v; \mu))_{k \in \mathbb{K}} \in \mathbb{R}^K.$$

To facilitate further discussion, we define the operators

$$\mathcal{S} : V_h^K \rightarrow \mathbb{R}, \quad u \mapsto \left(\Delta t \sum_{k=1}^K \|u^k\|_{V_h}^2 \right)^{1/2},$$

$$\mathcal{T} : (V_h')^K \rightarrow \mathbb{R}, \quad f(\cdot) \mapsto \left(\Delta t \sum_{k=1}^K \|f^k(\cdot)\|_{V_h'}^2 \right)^{1/2}.$$

Before defining a posteriori error estimators for \mathcal{J}_{RB} and $\nabla_{\mu} \mathcal{J}_{\text{RB}}$, estimators for the reduced solutions must be established.

Lemma 3.3 (Error Bounds). Let the trajectory $u \in Q_{\Delta t}^{\text{pr}}(0, T; V_{\text{RB}})$ be given and let $p(u; \mu) \in Q_{\Delta t}^{\text{ad}}(0, T; V_{\text{RB}})$ solve (8) for $\mu \in \mathcal{P}$ and the right-hand side defined by u . Furthermore, let $u_h(\mu) \in Q_{\Delta t}^{\text{pr}}(0, T; V_h)$ and $p_h(\mu) \in Q_{\Delta t}^{\text{ad}}(0, T; V_h)$ be the high-fidelity solutions obtained by the FOM. We then have for $e_{\text{pr}}(\mu) := u_h(\mu) - u(\mu)$ and $e_{\text{ad}}(\mu) := p_h(\mu) - p(u; \mu)$

$$\mathcal{S}(e_{\text{pr}}(\mu)) \leq \Delta^{\text{pr}}(u, \mu) := \alpha_{\text{LB}}^{-1}(\mu) \mathcal{T}(r_{\text{pr}}(u, \cdot; \mu)) \quad (9)$$

and

$$\mathcal{S}(e_{\text{ad}}(\mu)) \leq \Delta^{\text{ad}}(u, \mu) := \alpha_{\text{LB}}^{-1}(\mu) \left(8\gamma_d^2 (\Delta^{\text{pr}}(u, \mu))^2 + 2\mathcal{T}^2(r_{\text{ad}}(u, p(u; \mu), \cdot; \mu)) \right)^{\frac{1}{2}}. \quad (10)$$

Proof See Lemma 8 in [19] and apply the Cauchy-Schwarz inequality. \square

Given $\Delta^{\text{pr}}(u, \mu)$ and $\Delta^{\text{ad}}(u, \mu)$ for $u \in Q_{\Delta t}^{\text{pr}}(0, T; V_{\text{RB}})$, the errors of the associated RB objective functional and its gradient can be derived as follows.

Theorem 3.4 (A posteriori objective error estimates). For $\mu \in \mathcal{P}$, let the high-fidelity cost functional \mathcal{J}_h and the RB approximation \mathcal{J}_{RB} be defined as in (5) and Definition 3.1. Then, the following bounds hold:

$$|\mathcal{J}_h(\mu) - \mathcal{J}_{\text{RB}}(\mu)| \leq \Delta^{\mathcal{J}_{\text{RB}}}(\mu),$$

and

$$|d_{\mu_i} \mathcal{J}_h(\mu) - d_{\mu_i} \mathcal{J}_{\text{RB}}(\mu)| \leq \Delta^{d_{\mu_i} \mathcal{J}_{\text{RB}}}(\mu),$$

for $i \in \{1, \dots, P\}$, where the right-hand sides are given by

$$\Delta^{\mathcal{J}_{\text{RB}}}(\mu) := \mathcal{T}(r_{\text{ad}}(u_{\text{RB}}(\mu), p_{\text{RB}}(\mu), \cdot; \mu)) \Delta_{\text{RB}}^{\text{pr}}(\mu) + \gamma_d \Delta_{\text{RB}}^{\text{pr}}(\mu)^2$$

and

$$\begin{aligned} \Delta^{d_{\mu_i} \mathcal{J}_{\text{RB}}}(\mu) := & \mathcal{T}(f_{\mu_i}(\cdot; \mu)) \Delta_{\text{RB}}^{\text{ad}}(\mu) + \gamma_{a_{\mu_i}}^{\text{UB}}(\mu) \Delta_{\text{RB}}^{\text{pr}}(\mu) \Delta_{\text{RB}}^{\text{ad}}(\mu) \\ & + \gamma_{a_{\mu_i}}^{\text{UB}}(\mu) \Delta_{\text{RB}}^{\text{pr}}(\mu) \mathcal{S}(p_{\text{RB}}(\mu)) + \gamma_{a_{\mu_i}}^{\text{UB}}(\mu) \Delta_{\text{RB}}^{\text{ad}}(\mu) \mathcal{S}(u_{\text{RB}}(\mu)), \end{aligned}$$

where we define $\Delta_{\text{RB}}^{\text{pr}}(\mu) := \Delta^{\text{pr}}(u_{\text{RB}}(\mu), \mu)$, $\Delta_{\text{RB}}^{\text{ad}}(\mu) := \Delta^{\text{ad}}(u_{\text{RB}}(\mu), \mu)$, as well as $\mathcal{T}(f_{\mu_i}(\cdot; \mu)) := \mathcal{T}((f_{\mu_i}(\cdot; \mu))_{k \in \mathbb{K}})$.

Proof The proof follows analogously from [19, Theorems 9 and 10]. Unlike [19], we omit the last summand in the definition of $\Delta^{\mathcal{J}_{\text{RB}}}(\mu)$:

$$\Delta t \left| \sum_{k=1}^K r_{\text{pr}}^k(u_{\text{RB}}^k(\mu), p_{\text{RB}}^k(\mu); \mu) \right|. \quad (11)$$

This term is omitted since we restrict ourselves to a RB approach where the reduced primal and adjoint problem share identical vector spaces, ensuring that (11) is always zero. \square

Remark 3.5. If the high-fidelity solutions $u_h(\mu)$ and $p_h(\mu)$ belong to V_{RB} , then the RB approximations solving (7) and (8) coincide with them. Consequently, we obtain $\Delta^{\mathcal{J}}(\mu) = 0$ and $\Delta^{\nabla_{\mu} \mathcal{J}}(\mu) := (\Delta^{d_{\mu_1} \mathcal{J}_{\text{RB}}}(\mu), \dots, \Delta^{d_{\mu_P} \mathcal{J}_{\text{RB}}}(\mu)) = 0$.

3.2 RB Space Construction

We now discuss constructing a suitable basis for V_{RB} . The objective here is to maintain the smallest possible dimension while accurately approximating high-fidelity solutions for all parameter values. The basis of V_{RB} is expanded only when the approximation error for a queried parameter $\tilde{\mu}$, determined by the aforementioned estimators, exceeds a prescribed tolerance. In such cases, an adaptation procedure updates V_{RB} and the RB-ROM. The common approach utilizes high-fidelity trajectories for selected parameters (*snapshots*) to construct the RB space, ensuring accurate RB solutions (see Remark 3.5).

Given a potentially uninitialized (i.e., the basis may be empty) reduced space V_{RB} , the adaptation process at $\tilde{\mu} \in \mathcal{P}$ is as follows.

Procedure 3.6.

1. Solve the FOM at $\tilde{\mu}$ to obtain the primal and adjoint trajectories $u_h(\tilde{\mu})$ and $p_h(\tilde{\mu})$. Define

$$\mathcal{S}^{\text{pr}} := [u_h^1(\tilde{\mu}) - \Pi_{V_{\text{RB}}} u_h^1(\tilde{\mu}) \mid \dots \mid u_h^K(\tilde{\mu}) - \Pi_{V_{\text{RB}}} u_h^K(\tilde{\mu})] \in \mathbb{R}^{N_h \times K},$$

where $\Pi_{V_{\text{RB}}}$ is the $\langle \cdot, \cdot \rangle_{V_h}$ -projection into V_{RB} . The adjoint trajectory defines \mathcal{S}^{ad} analogously.

2. Apply the HaPOD [10] separately to \mathcal{S}^{pr} and \mathcal{S}^{ad} , generating sets of $\langle \cdot, \cdot \rangle_{V_h}$ -orthogonal vectors $\Phi^{\text{pr}} := \{\varphi_1^{\text{pr}}, \dots, \varphi_r^{\text{pr}}\}$ and $\Phi^{\text{ad}} := \{\varphi_1^{\text{ad}}, \dots, \varphi_r^{\text{ad}}\}$, satisfying

$$\sum_{s \in \mathcal{S}^{\text{pr}}} \|s - \Pi_{\text{span}\{\varphi_1^{\text{pr}}, \dots, \varphi_r^{\text{pr}}\}} s\|_{V_h}^2 < \epsilon_{\text{pod}}, \quad \sum_{s \in \mathcal{S}^{\text{ad}}} \|s - \Pi_{\text{span}\{\varphi_1^{\text{ad}}, \dots, \varphi_r^{\text{ad}}\}} s\|_{V_h}^2 < \epsilon_{\text{pod}}.$$

3. Extend V_{RB} with Φ^{pr} and Φ^{ad} , followed by reorthogonalization, defining an updated V_h -orthogonal basis, with dimension \tilde{N}_{RB} .
4. Precompute and store all parameter-independent properties. This includes $(\phi_i, \phi_j)_{L^2(\Omega)}$, $a^q(\phi_i, \phi_j)$ and $f^{\tilde{q}}(\phi_i)$, with $q \in Q_a$ and $\tilde{q} \in Q_f$ for all $i, j \in \{1, \dots, \tilde{N}_{\text{RB}}\}$ and for both projected PDEs as well as the Riesz-representatives used in the error estimator (9) and (10). The precomputation is carried out as described in [39], by projecting the operator in the residual to an approximate image basis. However, unlike [39], we omit orthogonalization for this basis to reduce the computational burden of the offline calculations.

The precomputations in Step 4 significantly reduce the online computational cost for parameter inference. This separation of parameter-independent and parameter-dependent computations is known as *offline/online decomposition*. Notably, for any tolerance ϵ_{POD} , the sets Φ^{pr} and Φ^{ad} in Step 2 can be chosen to satisfy the required accuracy constraints, ensuring that high-fidelity solutions and their RB approximations match at $\tilde{\mu}$ up to machine precision when ϵ_{POD} is appropriately selected.

4 Machine learning surrogates

Although RB methods are a powerful technique for reducing computational complexity, solving the PDE-constraint and adjoint problem remains a significant bottleneck, particularly for problems on long time scales. One strategy to enhance the RB approach, as discussed in, e.g., [21, 23, 40], involves replacing the RB-ROM with machine learning surrogate models which approximate the RB solution operator using a (supervised) Machine Learning (ML) algorithm. ML is a vast and rapidly evolving field, especially over the last decade. Here, we provide a concise and general introduction and refer the reader to the extensive literature for further details, e.g., [41–44].

Let \mathcal{X} and \mathcal{Y} be measurable spaces, and let $\mathcal{M}(\mathcal{X}, \mathcal{Y})$ denote the set of measurable functions mapping from \mathcal{X} to \mathcal{Y} . In general terms, supervised machine learning aims to *learn* a function $T : \mathcal{X} \rightarrow \mathcal{Y}$ that approximates an (often unknown) target function $\tilde{T} :$

$\mathcal{X} \rightarrow \mathcal{Y}$. The learning process relies on a finite training dataset $\mathcal{M}_{\text{train}} \subseteq (\mathcal{X} \times \mathcal{Y})^{N_{\text{train}}}$, consisting of N input-output pairs $\mathcal{M}_{\text{train}} = \{(x_1, \tilde{T}(x_1)), \dots, (x_N, \tilde{T}(x_{N_{\text{train}}}))\}$. Based on this data, a machine learning algorithm selects a function from a hypothesis set $\mathcal{F} \subset \mathcal{M}(\mathcal{X}, \mathcal{Y})$ of admissible functions. The selected function should best fit the training data while capturing the global behavior of \tilde{T} . It is crucial to note that this does not necessarily mean minimizing the error on the training data; rather, the objective is to generalize well to unseen data.

Our goal is to learn the parameter-dependent coefficients of RB solutions. Let V_{RB} be as defined above, with $N_{\text{RB}} = \dim V_{\text{RB}}$. Define the primal RB solution operator:

$$A_{\text{RB}}^{\text{pr}} : \mathcal{P} \rightarrow Q_{\Delta t}^{\text{pr}}(0, T; V_{\text{RB}}^{\text{pr}}); \quad \mu \mapsto u_{\text{RB}}(\mu) = \left(\sum_{n=1}^{N_{\text{RB}}} \frac{u_{\text{RB}}^k(\mu)_n \psi_n}{k \in \{0, \dots, K\}} \right). \quad (12)$$

For any $\mu \in \mathcal{P}$, this operator returns the solution to (7). Our objective is to learn a function

$$T : \mathcal{P} \rightarrow \mathbb{R}^{(K+1)N_{\text{RB}}}$$

that directly maps parameters to approximative Degree of Freedom (DoF) vectors for all times and basis vectors, i.e.

$$\underline{u}_{\text{ML}}^k(\mu)_n := T(\mu)_{kN_{\text{RB}}+n}, \quad 0 \leq k \leq K, \quad 1 \leq n \leq N_{\text{RB}}. \quad (13)$$

This methodology corresponds to the time-vectorized layout described in [1]. Similar to the RB approach, we define an ML approximative objective functional. However, a key difference is in computing the gradient. While for the RB-ROM equation (4) applies to the reduced solutions of (7) and (8), this is generally not the case for ML approximations. The reason is that $u_{\text{ML}}(\mu)$ and $p_{\text{ML}}(\mu)$ do not exactly solve the reduced equations, which is a prerequisite for using the adjoint methodology [35, Section 1.6.1]. We therefore demand C^1 -regularity for $\mu \mapsto \underline{u}_{\text{ML}}^k(\mu)_n$ and choose an ML model appropriately, computing gradients directly via the chain rule.

Definition 4.1. Let $T : \mathcal{P} \rightarrow \mathbb{R}^{(K+1)N_{\text{RB}}}$ be a learned, continuously differentiable function, and define $\underline{u}_{\text{ML}}^k(\mu)_n$ as in (13). Assume that

$$\underline{u}_{\text{ML}_n}^0 \equiv 0 \text{ and } d_{\mu_i} \underline{u}_{\text{ML}_n}^0 \equiv 0 \text{ for } 1 \leq n \leq N_{\text{RB}}.$$

Then, the *ML approximative primal solution* is given by

$$u_{\text{ML}}(\mu) := \left(\sum_{n=1}^{N_{\text{RB}}} \frac{\underline{u}_{\text{ML}}^k(\mu)_n \psi_n}{k \in \{0, \dots, K\}} \right) \in Q_{\Delta t}^{\text{pr}}(0, T; V_{\text{RB}}). \quad (14)$$

The respective partial derivatives are defined as

$$d_{\mu_i} u_{\text{ML}}(\mu) = \left(\sum_{n=1}^{N_{\text{RB}}} d_{\mu_i} \underline{u_{\text{ML}}^k(\mu)}_n \psi_n \right)_{k \in \{0, \dots, K\}} \in Q_{\Delta t}^{\text{pr}}(0, T; V_{\text{RB}}). \quad (15)$$

The ML approximative objective functional, analogous to Definition 3.1, is given by

$$\mathcal{J}_{\text{ML}}(\mu) := J(u_{\text{ML}}(\mu); \mu).$$

Using the chain rule, the partial derivatives of $\mathcal{J}_{\text{ML}}(\mu)$ are

$$d_{\mu_i} \mathcal{J}_{\text{ML}}(\mu) = \Delta t \sum_{k=1}^K [2d(u_{\text{ML}}^k(\mu), d_{\mu_i} u_{\text{ML}}^k(\mu)) + l^k(d_{\mu_i} u_{\text{ML}}^k(\mu))] + \lambda d_{\mu_i} \mathcal{R}(\mu),$$

for $i \in \{1, \dots, P\}$, defining the ML-ROM.

4.1 Error Estimates for ML Surrogates

Similarly to the RB case, we aim to certify the ML-ROM by defining a posteriori error estimators that provide upper bounds for the model error between \mathcal{J}_{ML} , $\nabla_{\mu} \mathcal{J}_{\text{ML}}$, and their high-fidelity counterparts. Following Lemma 3.3, an a posteriori error bound for $u_{\text{ML}}(\mu)$, as defined in (14), can be established such that for all $\mu \in \mathcal{P}$, the following holds:

$$\mathcal{S}(e(\mu)) \leq \Delta^{\text{pr}}(u_{\text{ML}}(\mu), \mu) = \alpha_{\text{LB}}^{-1}(\mu) \mathcal{T}(r_{\text{pr}}(u_{\text{ML}}(\mu), \cdot; \mu)), \quad (16)$$

where $e(\mu) := u_h(\mu) - u_{\text{ML}}(\mu)$, and $u_h(\mu) \in Q_{\Delta t}^{\text{pr}}(0, T; V_h)$ is the primal solution obtained via the FOM.

Similarly, an a posteriori error bound can be formulated for $d_{\mu_i} u_{\text{ML}}(\mu)$ by adapting the proof of Lemma 3.3 in [19] and Proposition 4.1 in [37], see Appendix A.

Lemma 4.2. Let $u_h(\mu) \in Q_{\Delta t}^{\text{pr}}(0, T; V_h)$ be the high-fidelity solution to (1), and let $u_{\text{ML}}(\mu) \in Q_{\Delta t}^{\text{pr}}(0, T; V_h)$ be defined as in Definition 4.1, with derivative $d_{\mu_i} u_{\text{ML}}(\mu)$. Define $d_{\mu_i} u_h(\mu)$ as the (well-defined) Fréchet derivatives of $u_h(\mu)$. For $k \in \mathbb{K}$, set

$$\begin{aligned} \mathcal{R}_{\text{ML}}^k(v; \mu) &:= d_{\mu_i} r_{\text{pr}}^k(u_{\text{ML}}^k, v; \mu) - a(d_{\mu_i} u_{\text{ML}}^k(\mu), v; \mu) \\ &\quad - \frac{1}{\Delta t} (d_{\mu_i} u_{\text{ML}}^k(\mu) - d_{\mu_i} u_{\text{ML}}^{k-1}(\mu), v)_{L^2(\Omega)}, \end{aligned} \quad (17)$$

for all $v \in V_h$. Then, for all $i \in \{1, \dots, P\}$, we have

$$\mathcal{S}(d_{\mu_i} e(\mu)) \leq \Delta_{\text{ML}}^{d_{\mu_i} u}(\mu) := \alpha_{\text{LB}}^{-1}(\mu) (\mathcal{T}(\mathcal{R}_{\text{ML}}(\cdot; \mu)) + \gamma_{a_{\mu_i}}(\mu) \Delta_{\text{ML}}^{\text{pr}}(\mu)),$$

where we define $d_{\mu_i} e(\mu) := d_{\mu_i} u_h(\mu) - d_{\mu_i} u_{\text{ML}}(\mu)$, $\Delta_{\text{ML}}^{\text{pr}}(\mu) := \Delta^{\text{pr}}(u_{\text{ML}}(\mu), \mu)$ and $\mathcal{R}_{\text{ML}}(\cdot; \mu) := (\mathcal{R}_{\text{ML}}^k(\cdot; \mu))_{k \in \mathbb{K}} \in (V_h')^K$.

Using this lemma, an a posteriori error bound can be formulated for $\mathcal{J}_{\text{ML}}(\mu)$ and $\nabla_{\mu}\mathcal{J}_{\text{ML}}(\mu) := (d_{\mu_1}\mathcal{J}_{\text{ML}}(\mu), \dots, d_{\mu_P}\mathcal{J}_{\text{ML}}(\mu))$, similar to Theorem 3.4. The proof is presented in Appendix A.

Theorem 4.3. Let $\mu \in \mathcal{P}$, and let $\mathcal{J}_h(\mu)$, $d_{\mu_i}\mathcal{J}_h(\mu)$ be defined as in Theorem 3.4. Then, we have

$$|\mathcal{J}_h(\mu) - \mathcal{J}_{\text{ML}}(\mu)| \leq \Delta^{\mathcal{J}_{\text{ML}}}(\mu), \quad (18)$$

and

$$|d_{\mu_i}\mathcal{J}_h(\mu) - d_{\mu_i}\mathcal{J}_{\text{ML}}(\mu)| \leq \Delta^{d_{\mu_i}\mathcal{J}_{\text{ML}}}(\mu), \quad (19)$$

for all $i \in \{1, \dots, P\}$. The error bounds on the right-hand side are given by

$$\Delta^{\mathcal{J}_{\text{ML}}}(\mu) := [2\mathcal{S}(u_{\text{ML}}(\mu)) + \mathcal{S}(g_{\text{ref}}(\mu))] \gamma_d \Delta_{\text{ML}}^{\text{pr}}(\mu) + \gamma_d \Delta_{\text{ML}}^{\text{pr}}(\mu)^2,$$

and

$$\begin{aligned} \Delta^{d_{\mu_i}\mathcal{J}_{\text{ML}}}(\mu) &:= [2\Delta_{\text{ML}}^{\text{pr}}(\mu) + 2\mathcal{S}(u_{\text{ML}}(\mu)) + \mathcal{S}(g_{\text{ref}})] \gamma_d \Delta_{\text{ML}}^{d_{\mu_i}u}(\mu) \\ &\quad + 2\mathcal{S}(d_{\mu_i}u_{\text{ML}}(\mu)) \gamma_d \Delta_{\text{ML}}^{\text{pr}}(\mu). \end{aligned}$$

4.2 General Considerations

Replacing the computation of the RB solutions with their ML counterparts offers two main advantages. Firstly, parameter inference using the ML-ROM is typically significantly faster [1, 27] compared to the RB-ROM. Secondly, this approach allows for parallel computation since the solution $u_{\text{ML}}^k(\mu)_n$ at a given time step does not explicitly depend on previous time steps, enabling simultaneous calculation of all time steps. However, to efficiently use an ML-based model for an optimization task, several key aspects regarding the training process and the specific considerations of incorporating an ML model into a gradient descent type optimization algorithm must be addressed. In this section, we outline the requirements an ML algorithm must satisfy to be considered viable in this context. Due to the lack of a sufficiently developed analytic theory (to the best of our knowledge), our argumentation will be primarily heuristic.

First, we must consider the domain of ML models and its impact on training. As previously mentioned, the surrogate function T is selected based on the available training data. A critical consequence of this is that the approximation quality of T generally deteriorates significantly in regions of \mathcal{P} with low training data density. When applying this to an RB optimization algorithm, we encounter the challenge that obtaining sufficient training data for a globally accurate ML model requires evaluating the RB models for a sufficiently large set of training parameters $\mathcal{P}_{\text{train}}$, distributed *uniformly* in \mathcal{P} . However, this approach would lead to an impractically large $\mathcal{P}_{\text{train}}$ and, consequently, an excessive number of RB model evaluations, rendering offline computations infeasibly costly. This issue becomes even more pronounced as the parameter space dimension P increases, a phenomenon commonly referred to

as the *Curse of Dimensionality*. Furthermore, we must ensure that the RB models themselves remain globally accurate with respect to the high-fidelity models. This further increases offline computational costs, as the reduced basis space V_{RB} must be sufficiently enriched to achieve the desired accuracy globally.

To address this challenge, we propose an algorithmic framework incorporating localized ML models, following the hierarchical modeling approach outlined in [1, 45, 46], adapted specifically for optimization tasks. In this framework, a hierarchy of models is established in decreasing order of accuracy and (generally) increasing inference speed. The key idea is to always attempt the fastest model first, only resorting to slower, more accurate models when necessary. Results from more precise models are then leveraged to iteratively enhance the less accurate models. Specifically, our approach first evaluates the ML-ROM; if its output lacks sufficient accuracy, we proceed to the RB-ROM. Should this also prove inadequate, the Full Order Model is employed. The FOM solutions are subsequently used to refine V_{RB} , while the RB solutions serve as training data for the ML-ROM. Unlike the approach in [1, 46], where re-adaptation is guided by an a posteriori error estimate, our re-training process is triggered by a decay condition of the objective functional, as detailed in Section 5. A crucial distinction of our approach is that we do not employ a distinct offline and online phase but instead alternate between model improvement and evaluation. This eliminates the need for an expensive offline phase, such as generating training data for a globally accurate ML model. Instead, we start with coarse models and refine them dynamically using intermediate results, adapting them to the domain of interest, which often reduces computational complexity compared to a priori constructed models.

Following this dynamic adaptation strategy, ML models are trained only with RB solutions collected during the optimization process. Consequently, ML models are expected to be sufficiently accurate only near the optimization trajectory. This necessitates careful selection of the learning method and imposes additional requirements to ensure the surrogate model’s quality. First, the learning procedure must perform well with relatively few localized training data (I) and must converge rapidly to the learned function (II). The latter is particularly important because, due to localization, ML models generally require multiple retraining steps, and excessive training overhead could negate the computational speed advantage. Additionally, we impose an interpolation property requirement (III), ensuring that the learned function satisfies

$$\max_{i \in \{1, \dots, N_{\text{train}}\}} \|y_i - T_\eta(x_i)\|_{\mathcal{Y}} \leq \eta, \quad (20)$$

where $\|\cdot\|_{\mathcal{Y}}$ is an appropriate norm on \mathcal{Y} . This property, combined with the continuity provided by the C^1 -regularity condition (see Definition 4.1), ensures approximation accuracy in a small region surrounding the training inputs x_1, \dots, x_N . However, it should be noted that, in general, the size of the region where the ML surrogates remain sufficiently accurate cannot be estimated reliably.

5 Trust region multi-fidelity optimization

In this section, we present a Trust-Region algorithm that integrates both RB-ROMs and ML-ROMs. As previously discussed, the RB-ROM serves as the foundation, providing both training data and certification. Following the approach outlined in [19], the global optimization problem 2.1 is reformulated as a sequence of iteratively solved sub-problems:

$$\mu^{(i+1)} := \underset{\mu \in \mathcal{P}}{\operatorname{argmin}} \mathcal{J}^{(i)}(\mu) \quad \text{s.t.} \quad \mu \in T^{(i)}, \quad (21)$$

which are solved until a global convergence criterion is met. Here, $\mathcal{J}^{(i)}(\cdot)$ represents a local approximation of $\mathcal{J}(\cdot)$ for each iteration index $i \in \mathbb{I} := 0, \dots, I-1$, for $I \in \mathbb{N}_0 \cup \{\infty\}$. Let $M^{(i)}$ denote models that provide access to local approximations $\mathcal{J}^{(i)}(\cdot)$ and their gradients $\nabla_{\mu} \mathcal{J}^{(i)}(\cdot)$. These models are updated iteratively to adapt to the current trust region. To ensure global convergence, we assume that for each sub-problem (21), a sequence $\{\mu^{(i,l)}\}_{l=0}^{L^{(i)}}$ can be found beginning with $\mu^{(i,0)} := \mu^{(i)}$, such that

$$\mathcal{J}^{(i)}(\mu^{(i,l)}) \geq \mathcal{J}^{(i)}(\mu^{(i,l+1)}) \quad \text{for all } l \in 0, \dots, L^{(i)} - 1. \quad (22)$$

This ensures a monotonic decrease in the objective function, driving the optimization process towards convergence. The final iteration point is used as the starting point for the next sub-problem, i.e., $\mu^{(i+1)} := \mu^{(i,L^{(i)})}$.

However, condition (22) alone does not guarantee a global decrease in the objective function. We therefore require that

$$\mathcal{J}^{(i)}(\mu^{(i)}) \geq \mathcal{J}^{(i+1)}(\mu^{(i+1)}) \quad \text{for all } i \in \mathbb{I}. \quad (23)$$

To ensure (23), we impose the *error-aware sufficient decrease condition*, given by:

$$\mathcal{J}^{(i)}(\mu_{\text{AGC}}^{(i)}) \geq \mathcal{J}^{(i+1)}(\mu^{(i+1)}), \quad (24)$$

in addition to (22), where $\mu_{\text{AGC}}^{(i)} := \mu^{(i,1)}$ represents the Approximate generalized Cauchy point (AGC). If (24) holds, then (23) is ensured, and $\mu^{(i+1)}$ is accepted. Otherwise, the guess $\mu^{(i+1)}$ is rejected, and the i -th sub-problem is resolved with a shrunken trust region. To verify (24) without the expensive construction of $M^{(i+1)}$, we assume that for all $i \in \mathbb{I}$, error bounds $\Delta^{\mathcal{J},(i)}(\mu^{(i+1)})$ and $\Delta^{\nabla \mathcal{J},(i)}(\mu^{(i+1)})$ are available, satisfying

$$\left| \mathcal{J}^{(i)}(\mu) - \mathcal{J}(\mu) \right| \leq \Delta^{\mathcal{J},(i)}(\mu) \quad \text{and} \quad \|\nabla_{\mu} \mathcal{J}^{(i)}(\mu) - \nabla_{\mu} \mathcal{J}(\mu)\|_{\mathbb{R}^P} \leq \Delta^{\nabla \mathcal{J},(i)}(\mu).$$

With these error estimates, the error-aware sufficient decrease condition can be refined by checking the following sufficient condition:

$$\mathcal{J}^{(i)}(\mu^{(i+1)}) + \Delta^{\mathcal{J},(i)}(\mu^{(i+1)}) < \mathcal{J}^{(i)}(\mu_{\text{AGC}}^{(i)}), \quad (25)$$

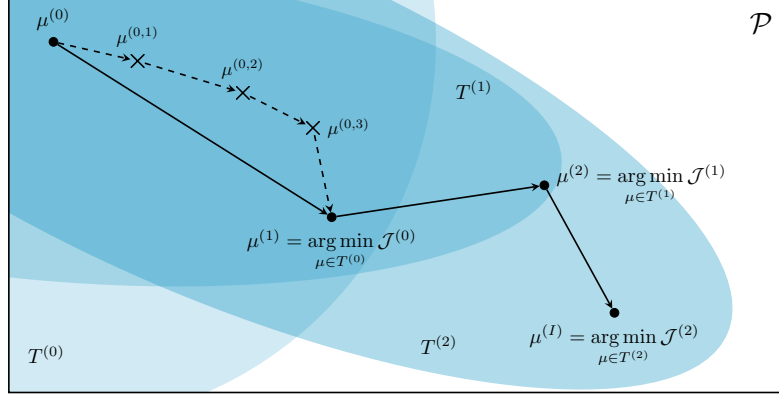


Figure 1: Schematic visualization of the abstract trust region algorithm.

and the necessary condition:

$$\mathcal{J}^{(i)}(\mu^{(i+1)}) - \Delta^{\mathcal{J},(i)}(\mu^{(i+1)}) \leq \mathcal{J}^{(i)}(\mu_{\text{AGC}}^{(i)}), \quad (26)$$

before going to (24), cf. [2]. The optimization process terminates when $\mu^{(i+1)}$ satisfies a *global first-order termination criterion*:

$$\|\mu^{(i+1)} - P_{\mathcal{P}}(\mu^{(i+1)} - \nabla_{\mu} \mathcal{J}(\mu^{(i+1)}))\|_{\mathbb{R}^P} \leq \tau, \quad (27)$$

where $\tau > 0$, cf. [3]. The operator $P : \mathbb{R}^P \rightarrow \mathcal{P}$ projects a potential overshoot back into the admissible domain, i.e.,

$$P(\mu)_j := \begin{cases} L_j, & \text{if } (\mu)_j \leq L_j, \\ (\mu)_j, & \text{if } L_j \leq (\mu)_j \leq U_j, \\ U_j, & \text{if } (\mu)_j \geq U_j. \end{cases}$$

All these elements together constitute the TR procedure we employ, as sketched in Figure 1 and detailed in Algorithm 1.

Remark 5.1. Algorithm 1 does not guarantee termination, as the optimization process may become trapped in an infinite loop, continuously rejecting each candidate $\mu^{(i+1)}$ due to the condition specified in line 14. However, if the algorithm does terminate, it can be shown that, under mild assumptions on $M^{(i)}$, the final iterate $\mu^{(I)}$ is, up to a given tolerance, a first-order critical point of \mathcal{J} , cf. [2]. In the following sections, we introduce suitable models $M^{(i)}$ that satisfy these conditions.

5.1 Backtracking Procedure

We will use the FOM defined in Section 3 as the model, providing access to $\mathcal{J}(\mu)$ and its gradient $\nabla_{\mu} \mathcal{J}(\mu)$, i.e., $\mathcal{J}(\mu) := \mathcal{J}_h(\mu)$ and $\nabla_{\mu} \mathcal{J}(\mu) := \nabla_{\mu} \mathcal{J}_h(\mu)$. It remains

Algorithm 1: Trust region optimization [2, 19]

```

1 Choose  $\mu^{(0)} \in \mathcal{P}$ , set  $i := 0$  and initialize  $M^{(0)}$ .
2 while (27) is not satisfied do
3   Compute  $\mu^{(i+1)}$  as solution of (21) with a convenient termination criteria.
4   if the sufficient condition (25) holds then
5     Accept  $\mu^{(i+1)}$ .
6     Use  $\mu^{(i+1)}$  to update the model  $M^{(i)}$ , getting  $M^{(i+1)}$  and set
7      $T^{(i+1)} := T^{(i)}$ .
8   else if condition (26) fails then
9     Reject  $\mu^{(i+1)}$  and shrunk  $T^{(i)}$ , getting  $T^{(i+1)} \subset T^{(i)}$ .
10  else
11    Use  $\mu^{(i+1)}$  to update the model  $M^{(i)}$ , getting  $M^{(i+1)}$ .
12    if (24) holds then
13      Accept  $\mu^{(i+1)}$  and set  $T^{(i+1)} := T^{(i)}$ .
14    else
15      Reject  $\mu^{(i+1)}$  and shrunk  $T^{(i)}$ , getting  $T^{(i+1)} \subset T^{(i)}$ .
16   $i \leftarrow i + 1$ 

```

to discuss the construction of the models $M^{(i)}$ and, based on this, the procedure for computing the sequence $\{\mu^{(i,l)}\}_{l=0}^{L^{(i)}}$. These aspects are closely interdependent, particularly when employing ML-ROM approaches. As outlined in Section 4, the ML surrogate requires continuous retraining, and its accuracy is therefore dependent on the parameters evaluated in previous iterations.

The algorithm we propose, is based on the projected BFGS method for simple bounded domains, as introduced in [3, 47]. The minimizing sequence $\{\mu^{(i,l)}\}_{l=0}^{L^{(i)}}$ is iteratively constructed, starting at $\mu^{(i,0)} := \mu^{(i)}$, using a backtracking procedure. For now, assume that for all $i \in \mathbb{N}_0$ and $\mu \in \mathcal{P}$, the function $\mathcal{J}^{(i)}(\mu)$ and its gradient $\nabla_{\mu} \mathcal{J}^{(i)}(\mu)$ are accessible. We define the update step as

$$\mu^{(i,l)}(k) := P \left(\mu^{(i,l)} + \alpha_0^{(i)} \kappa_{\text{bt}}^k d^{(i,l)} \right) \text{ for } k \in \mathbb{N}_0, \quad (28)$$

where $d^{(i,l)}$ denotes a descent direction at $\mu^{(i,l)}$, $\alpha_0^{(i)} > 0$ is the initial step size, and $\kappa_{\text{bt}} \in (0, 1)$ is a factor controlling the backtracking speed. The next iterate $\mu^{(i,l+1)}$ is selected as $\mu^{(i,l+1)} := \mu^{(i,l)}(\tilde{k})$, where $\tilde{k} \in \mathbb{N}_0$ is chosen to ensure sufficient decrease in $\mathcal{J}^{(i)}$. This decrease is enforced by verifying an Armijo-type condition:

$$\mathcal{J}^{(i)}(\mu^{(i,l)}) - \mathcal{J}^{(i)}(\mu^{(i,l)}(\tilde{k})) \geq \frac{\alpha_{\text{arm}}^{(i)}}{\alpha_0^{(i)} \kappa_{\text{bt}}^{\tilde{k}}} \|\mu^{(i,l)} - \mu^{(i,l)}(\tilde{k})\|_{\mathbb{R}^P}^2, \quad (29)$$

where $\alpha_{\text{arm}} = 10^{-6}$. Additionally, it must be ensured that $\mu^{(i,l)}(k)$ remains inside the trust region $T^{(i)}$ and that a minimum step size is satisfied to prevent unreasonably slow convergence. Hence, \tilde{k} is chosen as the smallest natural number (starting from zero) satisfying (29),

$$\|\mu^{(i,l)} - \mu^{(i,l)}(\tilde{k})\|_{\mathbb{R}^P} \geq \epsilon_{\text{cutoff}} \text{ and} \quad (30)$$

$$\mu^{(i,l)}(\tilde{k}) \in T^{(i)}, \quad (31)$$

for a given $\epsilon_{\text{cutoff}} > 0$. The iteration terminates when $\mu^{(i+1)} = \mu^{(i,L^{(i)})}$ satisfies the *sub-problem termination criterion* for some $\tau_{\text{sub}} \in (0, 1)$ and $\tau_{\text{sub}} \leq \tau$, i.e.

$$\|\mu^{(i,l)} - P_{\mathcal{P}}(\mu^{(i,l)} - \nabla_{\mu} \mathcal{J}^{(i)}(\mu^{(i,l)}))\| \leq \tau_{\text{sub}}. \quad (32)$$

The search directions $d^{(i,l)}$ are determined using the algorithm presented in [47, Section 5.5.3], given by

$$\tilde{d}^{(i,l)} := \begin{cases} -\tilde{\mathcal{H}}^{(i,l)} \nabla_{\mu} \mathcal{J}^{(i)}(\mu^{(i,l)}), & \text{if } -\nabla_{\mu} \mathcal{J}^{(i)}(\mu^{(i,l)})^T \tilde{\mathcal{H}}^{(i,l)} \nabla_{\mu} \mathcal{J}^{(i)}(\mu^{(i,l)}) < 0, \\ -\nabla_{\mu} \mathcal{J}^{(i)}(\mu^{(i,l)}), & \text{otherwise.} \end{cases} \quad (33)$$

If $\|\tilde{d}^{(i,l)}\| \neq 0$, we normalize $d^{(i,l)} := \tilde{d}^{(i,l)} / \|\tilde{d}^{(i,l)}\|$; otherwise, we set $d^{(i,l)} = 0$. The matrix $\tilde{\mathcal{H}}^{(i,l)}$ is an iteratively constructed approximation of the inverse Hessian $(\mathcal{H}_{\mathcal{J}}(\mu^{(i,l)}))^{-1}$, leveraging previously computed gradients $\nabla_{\mu} \mathcal{J}^{(i)}$, where the initialization is given by $\tilde{\mathcal{H}}^{(i,0)} := \text{Id}_{\mathbb{R}^P}$.

It is important to emphasize that the sequence $\{\mu^{(i,l)}\}_{l=0}^{L^{(i)}}$ defined by equations (29)–(32) is not necessarily well-defined. Specifically, for all $i \in \mathbb{N}_0$, the existence of a \tilde{k} satisfying (29)–(31) cannot be guaranteed. Moreover, it cannot be assumed that $\mathcal{J}^{(i)}$ possesses a first-order critical point within $T^{(i)}$, nor that any iterate $\mu^{(i,l)}$ satisfies the termination criterion (32). Therefore, it is essential for the final algorithm to incorporate mechanisms that handle these exceptions while ensuring that the sequence adheres to the decay condition (22).

5.2 RB-ML-ROM-optimization

Analogous to [3, 19], the RB space remains fixed for each sub-problem (21) and is updated in the outer loop (Algorithm 1; lines 6 and 10) using Procedure 3.6. This update is applied at $\mu^{(i+1)}$ by obtaining high-fidelity trajectories for $\mu^{(i+1)}$ and selecting relevant modes via the HaPOD-Greedy scheme. Given a fixed reduced space, we define the i -th RB surrogate model $M_{\text{RB}}^{(i)}$ as follows.

Definition 5.2. Let $i \in \mathbb{I}$ and $V_{\text{RB}}^{(i)}$ be given. The RB surrogate model $M_{\text{RB}}^{(i)}$ is characterized by the following components:

(I) **Evaluation of the Objective:**

$$\mathcal{J}_{\text{RB}}^{(i)}(\mu), \nabla_{\mu} \mathcal{J}_{\text{RB}}^{(i)}(\mu) \leftarrow M_{\text{RB}}^{(i)}. \text{eval_output}[\mu]$$

This method computes the RB approximate cost functional and its gradient (as per Definition 3.1) by solving (7) and (8) in $V_{\text{RB}}^{(i)}$.

(II) **Error Estimation:**

$$\Delta \mathcal{J}_{\text{RB}}^{(i)}(\mu), \Delta \nabla_{\mu} \mathcal{J}_{\text{RB}}^{(i)}(\mu) \leftarrow M_{\text{RB}}^{(i)}. \text{est_output}[\mu]$$

This method provides error estimates associated with $M_{\text{RB}}^{(i)}. \text{eval_output}[\mu]$, as defined in Theorem 3.4.

(III) **Model Extension:**

$$M_{\text{RB}}^{(i+1)} \leftarrow M_{\text{RB}}^{(i)}. \text{extend}[\mu]$$

A new surrogate model $M_{\text{RB}}^{(i+1)}$ is constructed by extending the RB space $V_{\text{RB}}^{(i)}$ according to Procedure 3.6. That is, $M_{\text{RB}}^{(i+1)}$ is analogous to $M_{\text{RB}}^{(i)}$ but utilizes an expanded space $V_{\text{RB}}^{(i+1)} \supset V_{\text{RB}}^{(i)}$.

Additionally, we define the training dataset:

(IV) **Training Data Collection:**

$$\mathcal{M}_{\text{train}} := ((\mu_1, \underline{u}_{\text{RB}}(\mu_1)), \dots, (\mu_{N_{\text{train}}}, \underline{u}_{\text{RB}}(\mu_{N_{\text{train}}}))$$

This set stores the DoF vectors from the last N_{train} computed solutions, where: $\underline{u}_{\text{RB}}(\mu) := (u_{\text{RB}}^k(\mu))_{k \in \{0, \dots, K\}}$.

By initializing $V_{\text{RB}}^{(0)} := \langle \emptyset \rangle$, we explicitly define the sequence of RB surrogate models $(M_{\text{RB}}^{(i)})_{i \in \mathbb{I}}$. Each sub-problem is uniquely associated with a surrogate model $M_{\text{RB}}^{(i)}$, which is iteratively refined using high-fidelity solutions obtained from previous sub-problems. Notably, the FOM for these solutions is evaluated only in the outer loop (Algorithm 1).

In contrast, a corresponding ML-based surrogate model requires frequent adaptation during solving the sub-problems, as discussed in Section 4. We now define the m -th ML surrogate model for the i -th sub-problem:

Definition 5.3. Let $i \in \mathbb{I}$, $m \in \mathbb{N}$, and let $M_{\text{RB}}^{(i)}$ be given as defined in Definition 5.2, with $N_{\text{RB}}^{(i)} := \dim V_{\text{RB}}^{(i)}$. The ML surrogate model $M_{\text{ML}}^{(i,m)}$ is defined as follows:

(I) **Learned Operator:**

$$T^{(i,m)} : \mathcal{P} \rightarrow \mathbb{R}^{(K+1)N_{\text{RB}}^{(i)}}$$

This operator maps μ to $(u_{\text{ML}}^k(\mu))_{k \in \{0, \dots, K\}}$, satisfying the conditions stated in Definition 4.1.

(II) **Evaluation of the Objective:**

$$\mathcal{J}_{\text{ML}}^{(i,m)}(\mu), \nabla_{\mu} \mathcal{J}_{\text{ML}}^{(i,m)}(\mu) \leftarrow M_{\text{ML}}^{(i,m)}. \text{eval_output}[\mu]$$

This method computes the ML approximation of the objective functional and gradient (as per Definition 4.1) by invoking $T^{(i,m)}$.

(III) **Model Training:**

$$M_{\text{ML}}^{(i,m+1)} \leftarrow M_{\text{ML}}^{(i,m)}. \text{train}$$

This method retrains $T^{(i,m)}$ using a ML algorithm on the dataset $\mathcal{M}_{\text{train}}$ collected by $M_{\text{RB}}^{(i)}$, yielding an updated model $T^{(i,m+1)}$. If $\mathcal{M}_{\text{train}}$ remains unchanged since the last training call, this training is skipped to avoid unnecessary computational overhead.

These models are initialized by setting $T^{(i,0)}$ as the zero operator. Although error estimators for the ML-ROM were derived in Section 4.1, they are not used to define $M_{\text{ML}}^{(i,m)}$. The primary reason is that, despite their theoretical value, these estimators are computationally inefficient due to the high inference speed of the ML models. Their use would significantly increase computational costs, potentially negating the speed advantage of the ML-ROM. Consequently, the models $M_{\text{ML}}^{(i,m)}$ remain *uncertified*, posing a challenge for direct application in a TR algorithm, as done in [3, 19]. In those approaches, the trust region is given as

$$\tilde{T}^{(i)} := \left\{ \mu \in \mathcal{P} \mid \Delta_r^{\mathcal{J}_{\text{RB}}^{(i)}}(\mu) \leq \epsilon_L^{(i)} \right\}, \quad (34)$$

for some $\epsilon_L^{(i)} > 0$, where $\Delta_r^{\mathcal{J}_{\text{RB}}^{(i)}}(\mu) := |\Delta^{\mathcal{J}_{\text{RB}}^{(i)}}(\mu) / \mathcal{J}_{\text{RB}}^{(i)}(\mu)|$. This formulation is not well suited for the machine learning surrogate. To address this limitation, we extend the trust region by introducing a *relaxation range* of width $\kappa^{(i)} := \alpha_0^{(i)} l_{\text{check}}$, where $l_{\text{check}} \in \mathbb{N}$, leading to the modified trust region

$$T^{(i)} := \left(\tilde{T}^{(i)} \cup \bigcup_{\mu \in \partial \tilde{T}^{(i)}} \left\{ \tilde{\mu} \in \mathbb{R}^P \mid \|\tilde{\mu} - \mu\|_{\mathbb{R}^P} \leq \kappa^{(i)} \right\} \right) \cap \mathcal{P}.$$

This construction eliminates the need to verify condition (31) at each backtracking step. If $\Delta_r^{\mathcal{J}_{\text{RB}}^{(i)}}(\mu^{(i,n)}) \leq \epsilon_L^{(i)}$ holds for some $n \in \mathbb{N}_0$, then

$$\mu^{(i,l)}(k) \in T^{(i)} \text{ for all } k \in \mathbb{N}_0 \text{ and } l \in \{n, \dots, n + l_{\text{check}}\}.$$

Thus, to ensure that $\mu^{(i,l)}$ remains inside the trust region for all $l \in \{0, \dots, L^{(i)}\}$, it suffices to check $\Delta_r^{\mathcal{J}_{\text{RB}}^{(i)}}(\mu^{(i,l)}) \leq \epsilon_L^{(i)}$ every l_{check} -th iteration in the inner loop. Thus, if $l \bmod l_{\text{check}} = 0$ hold, we call l a *checkpoint*. In addition to $\epsilon_L^{(i)}$, we define $\alpha_L^{(i)} > 0$, and demand $\alpha_0^{(i)} \leq \alpha_L^{(i)}$ for all $i \in \mathbb{I}$. If $\mu^{(i+1)}$ is not accepted, $T^{(i)}$ is shrunk by setting

$\epsilon_L^{(i+1)} := \beta_1 \epsilon_L^{(i)}$ for $\beta_1 \in (0, 1)$ and $\alpha_L^{(i+1)} := \beta_2 \alpha_L^{(i)}$ for $\beta_2 \in (0, 1)$. Otherwise, the trust region remains unchanged, i.e., $\epsilon_L^{(i+1)} := \epsilon_L^{(i)}$ and $\alpha_L^{(i+1)} := \alpha_L^{(i)}$.

Notably, alternative algorithms have already been proposed, cf. [5], that incorporate the idea of relaxing the trust region to allow larger errors in the inner loop, providing greater flexibility in model selection.

Remark 5.4. Beyond avoiding the computational cost of error estimation for the ML model, redefining the trust region has another significant advantage. Specifically, defining the trust region via $\Delta^{\mathcal{J}_{\text{ML}}}$ in a manner similar to (34) could lead to unnecessary expansions of the reduced basis, resulting in computational overhead [3–5].

Consider a scenario where the relative error of $\mathcal{J}_{\text{ML}}^{(i)}(\mu)$ exceeds the tolerance $\epsilon^{(i)}$, while the error for $\mathcal{J}_{\text{RB}}^{(i)}(\mu)$ remains below this threshold. If a trust region like $\tilde{T}^{(i)}$ were used, it would unnecessarily trigger a fallback to the main loop, leading to costly reconstruction of the reduced basis although the RB model itself remains adequate. Given the iterative retraining and volatile nature of $M_{\text{ML}}^{(i,m)}$, such cases are frequent but can typically be resolved by retraining $M_{\text{ML}}^{(i,m)}$, as long as the underlying RB space $V_{\text{RB}}^{(i)}$ remains sufficient.

With these considerations, we can now define the TR-RB-ML algorithm. Our goal is to build upon the approaches in [3, 19], using $M_{\text{RB}}^{(i)}$ and $M_{\text{ML}}^{(i,m)}$ to compute $\mathcal{J}^{(i)}(\mu)$ and $\nabla_{\mu} \mathcal{J}^{(i)}(\mu)$, depending on the state of the BFGS optimization procedure. We aim to rely on $M_{\text{ML}}^{(i,m)}$ as much as possible while using $M_{\text{RB}}^{(i)}$ only when necessary. Importantly, ML models will not be employed in the outer loop (Algorithm 1). All surrogate evaluations for conditions (24), (25), and (26) will be handled by $M_{\text{RB}}^{(i)}$. As discussed in Remark 5.4, this is crucial for determining whether a re-adaptation of $M_{\text{RB}}^{(i)}$ is required. Therefore, the outer loop remains as defined in Algorithm 1, while we modify how subproblems are solved in the inner loop (line 3 in Algorithm 1) to return $\mu^{(i)}$.

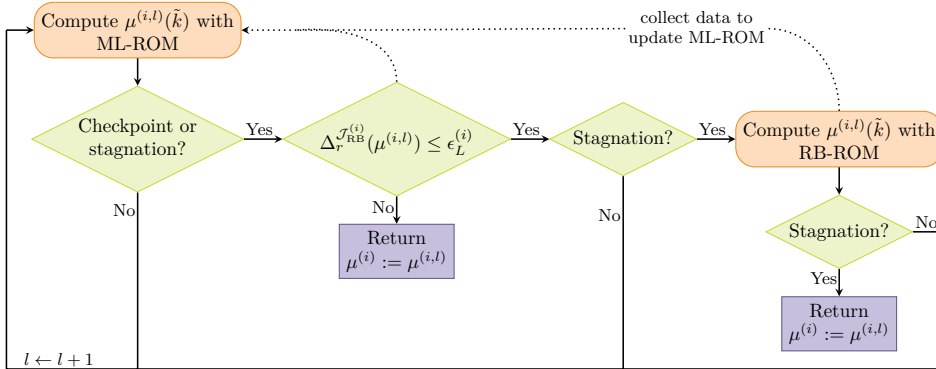


Figure 2: Simplified flowchart illustrating the inner loop of the relaxed TR-RB-ML algorithm, as described in Algorithm 1, after the warm-up phase.

During the first $l_{\text{warmup}} \in \mathbb{N}$ iterations of this inner loop, $M_{\text{RB}}^{(i)}$ is utilized to compute objective functional and gradient. This warm-up phase is necessary for accumulating a sufficient training dataset $\mathcal{M}^{\text{train}}$, which is essential for initializing valid ML models. Moreover, in the first iteration (beginning at $\mu^{(i)}$), the cutoff condition (30) is not enforced. As highlighted in [2], this ensures that a valid AGC $\mu^{(i,1)}$ will be found by the backtracking procedure, which is crucial for preventing stagnation of Algorithm 1 away from an optimum. In the remaining iterations, $M_{\text{ML}}^{(i,m)}$, trained on

Algorithm 2: Inner loop

```

1 Let  $\mu^{(i)}$  and the local surrogate models  $M_{\text{RB}}^{(i)}$  and  $M_{\text{ML}}^{(i,0)}$  be given.
2 Set  $l := 0$ ,  $\mu^{(i,0)} := \mu^{(i)}$ ,  $\epsilon^{(i)} > 0$ ,  $\tilde{\mathcal{H}}^{(i,0)} := \text{Id}_{\mathbb{R}^P}$ ,  $d^{(i,0)} := -\nabla_{\mu} \mathcal{J}^{(i)}(\mu^{(i,0)})$ ,
   no_progress := false and use_ML := true.
3  $\mathcal{J}^{(i)}(\mu^{(i,0)})$ ,  $\nabla_{\mu} \mathcal{J}^{(i)}(\mu^{(i,0)}) \leftarrow M_{\text{RB}}^{(i)}.eval\_output[\mu^{(i,0)}]$ 
4 while (32) is not satisfied or  $l = 0$  do
5   if  $l \bmod l_{\text{check}} = 0$  or no_progress then
6     if  $\Delta_r^{\mathcal{J}_{\text{RB}}^{(i)}}(\mu^{(i,l)}) > \epsilon_L^{(i)}$  then go to line 29.
7   Set  $k := 0$  and no_progress  $\leftarrow$  false.
8   while (29) is not satisfied do
9     Get  $\mu^{(i,l)}(k)$  by (28).
10    if  $l \leq l_{\text{warmup}}$  or not use_ML then
11       $\mathcal{J}^{(i)}(\mu^{(i,l)}(k))$ ,  $\nabla_{\mu} \mathcal{J}^{(i)}(\mu^{(i,l)}(k)) \leftarrow M_{\text{RB}}^{(i)}.eval\_output[\mu^{(i,l)}(k)]$ 
12    else
13       $\mathcal{J}^{(i)}(\mu^{(i,l)}(k))$ ,  $\nabla_{\mu} \mathcal{J}^{(i)}(\mu^{(i,l)}(k)) \leftarrow M_{\text{ML}}^{(i,m)}.eval\_output[\mu^{(i,l)}(k)]$ 
14    if not (30) and  $l > 0$  then
15      no_progress  $\leftarrow$  true
16      Go to line 18.
17     $k \leftarrow k + 1$ 
18  if no_progress and not use_ML then
19    Go to line 29.
20  else if no_progress then
21    use_ML  $\leftarrow$  false
22     $d^{(i,l)} \leftarrow -\nabla_{\mu} \mathcal{J}_{\text{RB}}^{(i)}(\mu^{(i,l)})$  and  $\tilde{\mathcal{H}}^{(i,l)} \leftarrow \text{Id}_{\mathbb{R}^P}$ .
23  else
24    use_ML  $\leftarrow$  true and no_progress  $\leftarrow$  false
25     $\mu^{(i,l+1)} := \mu^{(i,l)}(k)$ 
26    Get  $\mathcal{H}^{(i,l+1)}$  and  $d^{(i,l+1)}$  by (33).
27     $M_{\text{ML}}^{(i,m+1)} \leftarrow M_{\text{ML}}^{(i,m)}.train$ 
28     $l \leftarrow l + 1$  and  $m \leftarrow m + 1$ 
29 return  $\mu^{(i+1)} := \mu^{(i,l)}$ 

```

data previously collected by the RB model, will be used. In the case that for $\mu^{(i,l)}$ no sufficient $\mu^{(i,l)}(k)$ can be found, before reaching the minimum step size, i.e. (30) can not be not satisfied, the backtracking is stopped and it is checked that the last accepted parameter is still in the relaxed trust region, i.e. $\Delta_r^{\mathcal{J}_{\text{RB}}^{(i)}}(\mu^{(i,l)}) \leq \epsilon_L^{(i)}$. If this check fails, $\mu^{(i,l)}$ is returned as $\mu^{(i+1)}$ to the main loop. If the check succeeds, $\tilde{\mathcal{H}}^{(i,l)}$ is reset to $\text{Id}_{\mathbb{R}^P}$ and $d^{(i,l)}$ is updated to $-\nabla_{\mu} \mathcal{J}_{\text{RB}}^{(i)}(\mu^{(i,l)})$. The backtracking is then rerun, this time using the RB model $M_{\text{RB}}^{(i)}$, for all calculations. Note that, in general, the $M_{\text{RB}}^{(i)}$ is more accurate than $M_{\text{ML}}^{(i,m)}$, because the ML model depends on RB data, which introduces an additional model error. If this second attempt succeeds, the model $M_{\text{ML}}^{(i,m)}$ is retrained on the updated training sets that are derived by leveraging the RB model. Subsequent BFGS iterations proceed as before, utilizing the updated ML model $M_{\text{ML}}^{(i,m+1)}$. However, if again no $\mu^{(i,l)}(k)$ can be found satisfying (29) - (31), $\mu^{(i,l)}$ is also returned as $\mu^{(i+1)}$ and the RB space re-adapted.

As previously mentioned, we can ensure condition (31) by periodically verifying that the relative error of the RB model remains below $\epsilon^{(i)}$. This approach circumvents the necessity to check (31) for each $k \in \mathbb{N}_0$ and $l \in \{0, \dots, L^{(i)}\}$. Consequently, the relative error is evaluated every l_{check} -th iteration. If the error surpasses this threshold, the parameter $\mu^{(i,l)}$ is returned as $\mu^{(i+1)}$ to the main loop. The complete process of the inner loop computation is detailed in Algorithm 2. Combined with the outer loop procedure this defines the TR-RB-ML algorithm. Figure 2 shows a simplified flow chart, illustrating the key steps of the inner loop.

6 Numerical experiments

In this section, we apply the proposed algorithm to an example problem aimed at optimizing parameters for managing temperature distribution in a building. We compare its performance with established optimization algorithms to assess its effectiveness. Our objective is to evaluate the strengths and limitations of the proposed method and identify areas where further improvements appear necessary.

6.1 Problem

As a test case, we seek to determine the optimal heat conductivity values for structural elements (doors and walls) in a building floor $\Omega := (0, 2) \times (0, 1)$, as shown in Figure 3.

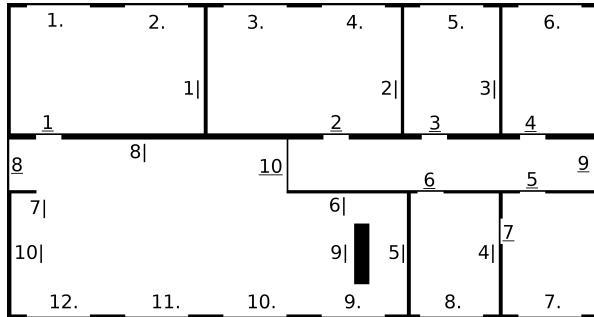


Figure 3: From [3]: On the floor with domain $\Omega := (0, 2) \times (0, 1)$ heaters below the windows i ., doors \underline{i} and walls $i|$ are places. Each has its own parameter μ_* describing the power of the heaters or respectively the heat conductivity of the components. Everywhere else the conductivity is fixed as $\mu_{\text{air}} = 0.5$.

The goal is to minimize the quadratic discrepancy between the actual temperature distribution $u(\mu)$ and a desired reference distribution g_{ref} . The temperature is governed by the instationary heat equation, where

$$a(u, v; \mu) := \int_{\Omega} \kappa(\mu) \nabla u(x) \nabla v(x) dx, \quad f(v; \mu) := \int_{\Omega} \eta(\mu) v(x) dx$$

for all $v \in V$. We impose homogeneous Dirichlet boundary conditions on $\partial\Omega$ and set the initial temperature distribution to $u^0(\mu) \equiv 0$. The parameters $\kappa(\mu)$ and $\eta(\mu)$ model the building components as linear combinations of indicator functions, specifying the locations and corresponding material properties. The diffusion coefficient $\kappa(\mu)$ governs the heat conductivity of walls and doors, while $\eta(\mu)$ in the source term represents the heating capacity, scaled by the function $b(t) := \min\{2t, 1\}$, which accounts for the time required for heaters to reach full power.

The outer walls and doors ($\mu_{10}, \mu_{\text{g}}, \mu_{\text{d}}$) have a prescribed heat conductivity of $5.0 \cdot 10^{-3}$, while the heating capacity of all heaters is fixed at 80. The remaining walls and doors are assigned common conductivity values, denoted by μ_{walls} and μ_{doors} , respectively. Our objective is to determine optimal values for these parameters within the range $[0.01, 0.1]$, i.e., $\mathcal{P} := [0.01, 0.1] \times [0.01, 0.1] \subset \mathbb{R}^2$. We define the function space $V := H_0^1(\Omega)$ and the inclusion operator $F : H_0^1(\Omega) \rightarrow L^2(\Omega)$, where $L^2(\Omega)$ is equipped with the inner product $\frac{10^4}{2}(\cdot, \cdot)_{L^2(\Omega)}$. A triangular spatial grid with 10,151 nodes ($\dim V_h = 10,151$) is used, along with a temporal grid consisting of 10,001 points ($K = 10,000$) with uniform time steps $\Delta t = 1/10$, forming the Full Order Model. The reference distribution $g_{\text{ref}} \in Q_{\Delta t}^{\text{pf}}(0, T; V_h)$ is obtained as the primal solution of the FOM for $\hat{\mu} := (0.05, 0.05)$. Regularization is imposed through a quadratic penalty on deviations from $\hat{\mu}$, with a weight of $\lambda = 0.5 \cdot 10^{-3}$. Consequently, the objective functional is given by

$$\mathcal{J}_h(\mu) = \frac{10^3}{2} \sum_{k=1}^K \|u_h^k(\mu) - g_{\text{ref}}^k\|_{L^2(\Omega)}^2 + \frac{10^{-3}}{2} \sum_{i=1}^P \|\mu_i - \hat{\mu}_i\|_{\mathbb{R}^P}^2.$$

Since this functional is convex, it guarantees the existence of a unique minimizer at $\hat{\mu}$.

6.2 Kernel methods

As outlined in Section 4, ML methods must satisfy certain criteria to be viable for optimization tasks. Selecting the optimal method involves balancing various properties. For instance, a Deep Neural Network (DNN) is generally unsuitable due to its over-parameterization, high data requirements, and lack of interpolation properties. Consequently, we employ a kernel-based model for our numerical experiments. Kernel methods are a mathematically well-studied field and widely applied in varying contexts including numerical mathematics, machine learning and many other areas. For a broader introduction, we refer to [48–50].

The surrogate function $T : \mathcal{P} \rightarrow \mathbb{R}^q$ (13) is constructed as a vector-valued linear combination of kernel functions centered at distinct training inputs $\mu_1, \dots, \mu_{N_{\text{train}}}$

with corresponding coefficients $\alpha_1, \dots, \alpha_{N_{\text{train}}} \in \mathbb{R}^q$:

$$T(\cdot) := \sum_{i=1}^{N_{\text{train}}} \alpha_i K(\cdot, \mu_i) \in \text{span} \{vK(\cdot, \mu_i) \mid i \in \{1, \dots, N_{\text{train}}\}, v \in \mathbb{R}^q\} =: \mathcal{F}. \quad (35)$$

Here, $q = (K + 1)N_{\text{RB}}^{(i)}$, where $N_{\text{RB}}^{(i)}$ denotes the dimension of the RB space on which the ML-ROM is defined. The kernel function $K : \mathcal{X} \times \mathcal{P} \rightarrow \mathbb{R}^{q \times q}$ is symmetric, i.e., $K(\mu, \tilde{\mu}) = K(\tilde{\mu}, \mu)^T$ for all $\mu, \tilde{\mu} \in \mathcal{P}$. Given training data $\{(\mu_1, y_1), \dots, (\mu_N, y_{N_{\text{train}}})\}$, the goal is to determine optimal coefficients $\alpha_1, \dots, \alpha_{N_{\text{train}}}$ such that $T(\mu_i) = y_i$ for all $i \in \{1, \dots, N_{\text{train}}\}$. This corresponds to solving the linear system:

$$A\alpha = y, \quad \text{where } \alpha := (\alpha_1, \dots, \alpha_{N_{\text{train}}}), \quad y := (y_1, \dots, y_{N_{\text{train}}}), \quad (36)$$

with the kernel matrix $A := (K(\mu_i, \mu_j))_{(i,j)} \in \mathbb{R}^{qN_{\text{train}} \times qN_{\text{train}}}$. If K is strictly positive definite, this system has a unique solution. Training the model thus reduces to solving this linear system, typically via numerical methods such as QR decomposition. To improve numerical stability, A is often regularized by adding $\eta \text{Id}_{\mathbb{R}^{qN_{\text{train}}}}$ for some $\eta > 0$, yielding:

$$(A + \eta \text{Id}_{\mathbb{R}^{qN_{\text{train}}}})\alpha = y. \quad (37)$$

If $K(\cdot, \mu_i)$ is continuously differentiable for all $i \in \{1, \dots, N_{\text{train}}\}$, then for sufficiently small η , the kernel-based ML model satisfies requirement (20). Furthermore, kernel methods inherently satisfy the initial conditions in Definition 4.1, i.e., $u_{\text{ML}_n}^0 \equiv 0$ and $d_{\mu_i} u_{\text{ML}_n}^0 \equiv 0$ for $1 \leq n \leq N_{\text{RB}}$, due to $u_{\text{RB}}^0 \equiv 0$ and the uniqueness of (37).

The training of such kernel methods is computationally efficient as long as the dataset size remains moderate. However, scalability issues arise with large datasets. In such cases, alternative approaches like Vectorial Kernel Orthogonal Greedy Algorithm (VKOGA) [50] can mitigate these challenges. In our case, we instead limit the training set to the most recent $N_{\text{train}} = 10$ evaluated parameters and their corresponding RB solutions. This ensures local accuracy near the current optimization trajectory while improving numerical stability, particularly when training data clusters within \mathcal{P} . It also allows for smaller regularization parameters, reducing interpolation error. For our experiments, we set $\eta = 10^{-12}$. Additionally, to further enhance numerical stability, training data is normalized to the range $[-1, 1]^2$.

A crucial factor in approximation quality is the choice of the kernel function. For our application, radial basis function (RBF) kernels are particularly effective. We employ a Gaussian kernel, i.e. $K(\mu_i, \mu_j) := e^{-0.01\|\mu_i - \mu_j\|_{\mathbb{R}^P}^2} \text{Id}_{\mathbb{R}^q}$, which is continuously differentiable for all $\mu_j \in \mathcal{P}$, with derivative

$$d_{\mu_i} K(\mu, \mu_j) = -2 \times 10^{-4} (\mu - \mu_j)_i e^{-0.01\|\mu_i - \mu_j\|_{\mathbb{R}^P}^2} \text{Id}_{\mathbb{R}^q}.$$

6.3 Methods used

We conduct four separate optimization experiments, each employing a different algorithm:

1. **FOM-Opt:** Optimization is performed using BFGS directly on the FOM, without a TR scheme.
2. **TR-RB-Opt:** Optimization follows a TR scheme with RB-ROM, as demonstrated by Qian et al. [19].
3. **Relaxed TR-RB-Opt:** The optimization algorithm described in Section 5 is applied, but using only the RB model for parameter inference, without the ML model.
4. **Relaxed TR-RB-ML-Opt:** Optimization follows the algorithm detailed in Section 5, incorporating the ML model.

All algorithms are implemented in `Python`, utilizing `pyMOR` [34] for discretization and model order reduction, including HaPOD. The kernel method implementation also leverages functions from VKOGA [50]. The source code is available at [51]. All computations were performed on a custom-built PC equipped with an AMD Ryzen 7 3700X 8-Core Processor (16 threads) and 96 GB RAM. The continuity and coercivity constants, or their respective bounds, were computed analogously to [19] using the *Riesz-eigenvalue approach* for γ_d and the *min-/max-theta method* for the bounds $\alpha_{\text{LB}}(\mu)$ and $\gamma_{a_{\mu_i}}^{\text{UB}}(\mu)$; see [19, 38] for details.

Across all experiments, the optimization termination tolerance is set to $\tau = 10^{-3}$. The backtracking step size decay factor is $\kappa_{\text{bt}} = 0.5$, with an initial step size of $\alpha_0^{(0)} = 10^{-3}$. For all trust-region-based algorithms (Experiments 2 – 4), the subproblem termination tolerance is set to $\tau_{\text{sub}} = 5 \cdot 10^{-4}$, while the initial relative error tolerance is $\epsilon_L^{(0)} = 0.1$, with a decay factor of $\beta_1 = 0.95$. For relaxed trust-region variants (Experiments 3 and 4), the relative error is checked every 25 steps ($l_{\text{check}} = 25$), with a minimum step size of $\epsilon_{\text{cutoff}} = 10^{-6}$. The initial maximum size is $\alpha_L^{(0)} = 0.01$, with a decreasing factor $\beta_2 = 0.95$. To generate training data and reinitialize the ML-ROM upon expanding the RB space, we set $l_{\text{warmup}} = 3$.

Since optimization behavior depends on the initial guess $\mu^{(0)}$, we conduct ten independent runs per experiment, with $\mu^{(0)}$ uniformly sampled from \mathcal{P} . These initial values remain consistent across all experiments to ensure comparability.

6.4 Results

All optimization runs successfully converge within the specified tolerance to the global minimum at $\bar{\mu} = (0.05, 0.05)$. An example is illustrated in Figure 4. Table 1 presents

Algorithm	Time [s]	Speed-up	FOM eval.	RB-ROM eval.	ML-ROM eval.
FOM-Opt	2550.20	–	68.40	–	–
TR-RB-Opt	911.65	2.80	7.50	154.60	–
Relaxed TR-RB-Opt	406.42	6.27	4.40	90.70	–
Relaxed TR-RB-ML-Opt	304.50	8.38	5.10	30.90	108.00

Table 1: Total runtime and number of evaluations for FOM, RB-ROM, and ML-ROM across selected algorithms, averaged over ten optimization runs with different initial guesses.

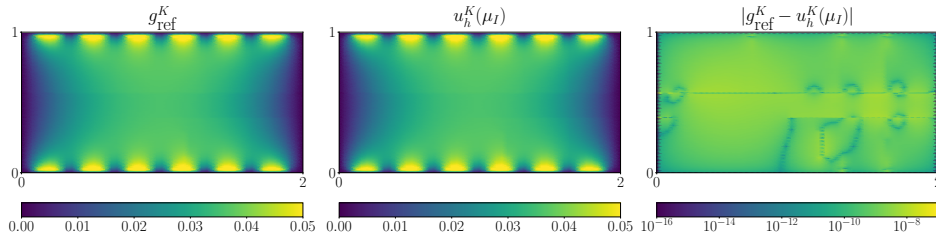


Figure 4: Comparison of the desired state g_{ref} (left), the final state obtained using the relaxed TR-RB-ML algorithm with initial guess $\mu^{(0)} = (0.026, 0.020)$ (middle), and their absolute differences (right) at the final time step ($K = 10000$).

the total runtimes and the number of model evaluations, averaged over ten optimization runs with varying initial guesses. All algorithms outperform the FOM variant in terms of computational efficiency. Notably, the relaxed TR-RB-ML approach achieves the most significant reduction in computation time, with a speed-up factor of 8.38. This result demonstrates that augmenting RB-ROM with ML-ROM can be a viable strategy for reducing computational costs.

This becomes even more evident when examining the evaluation times for individual queries in greater detail. Figure 5 illustrates the evaluation times for the optimization using the relaxed TR-RB method, starting at $\mu^{(0)} = (0.026, 0.020)$. The figure shows the time required to compute primal solutions and error estimates of the RB-ROM for each queried parameter. Most evaluations are carried out by ML-ROMs, while RB-ROMs are primarily used at the beginning of each subproblem iteration for collecting training data and towards the end of the optimization process, where they are used more frequently, due to the more accurate approximations. As expected, ML-ROM evaluations are significantly faster, up to a factor of 10^2 , compared to RB-ROM evaluations. Moreover, the effective online speed-up is even greater since gradients can be computed directly via the chain rule, whereas FOM and RB-ROM require additional calculations obtaining the adjoint solution.

Despite the impressive speed-up in individual parameter inferences, the overall speed-up is less pronounced, as shown in Table 1. This discrepancy arises because the optimization process includes several additional computationally intensive steps that remain unoptimized and do not benefit from ML-ROM acceleration.

The most time-consuming steps in the optimization process are FOM evaluations, required for constructing RB spaces, and RB-ROM evaluations, necessary for generating training data. In the relaxed TR-RB-ML optimization, ML-ROM evaluations contribute, on average, less than 0.04% of the total runtime, while FOM evaluations account for 54.44%, RB-ROM evaluations for 12.45%, and RB space construction for 12.69%. Another costly step is the initialization of the optimization setup, particularly the construction of the FOM. These findings align with previous studies [3, 4], which highlight the extension of the RB space as a critical performance bottleneck in TR approaches.

From Table 1, we observe that incorporating ML-ROM can sometimes negatively impact performance. Optimization runs using ML methods generally require more

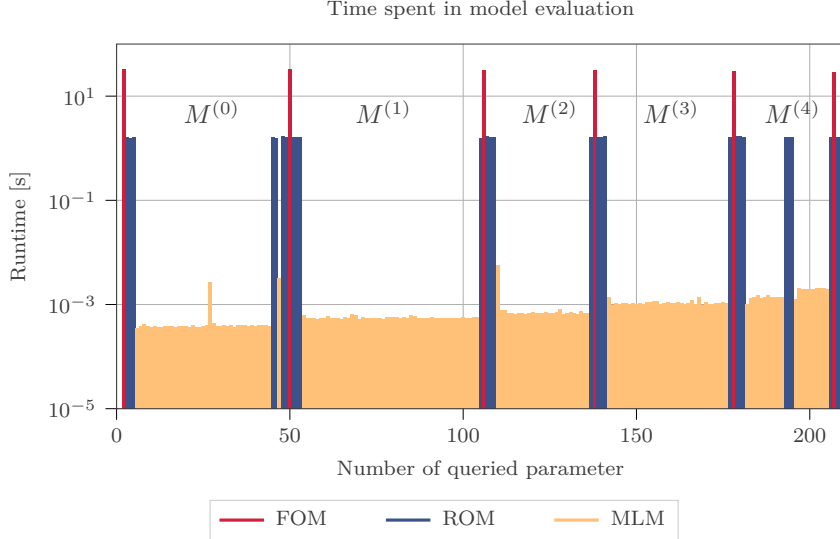


Figure 5: Evaluation times of the primal models for each queried parameter during the run performed by the relaxed TR-RB-ML algorithm, starting at $\mu^{(0)} = (0.026, 0.020)$. The colors indicate the model used: FOM (red), RB-ROM (blue), and ML-ROM (orange). Additionally, the scope of the RB-ROMs $M^{(i)}$ is shown.

FOM evaluations and, consequently, more RB space extensions compared to the relaxed TR-RB method without ML-ROM. This occurs because ML-ROMs typically exhibit higher errors than RB-ROMs, potentially leading to stagnation away from the optimum. Such stagnation triggers the check that $\mu^{(i,l)}$ is an element of $\tilde{T}^{(i)}$ (Line 6 in Algorithm 2), potentially resulting in more frequent fallbacks to the main loop. This also explains why total parameter evaluations increase when ML-ROM is incorporated, as seen in Table 1.

However, this also suggests that the observed speed-up cannot be entirely attributed to the incorporation of ML-ROMs. A major contributing factor to the reduced computation time for the relaxed TR-RB-ML optimization is the reduction in FOM evaluations due to the introduction of the relaxed trust region. This becomes particularly evident when comparing the speed-up factors of TR-RB-Opt (2.80) and relaxed TR-RB-Opt (6.27). A likely explanation is that the error estimators introduced in Section 3.1 tend to overestimate the actual error of RB solutions, imposing unnecessarily strict restrictions for convergence and prompting premature RB space reconstructions. An additional effect that further reduces computation time is the reduction in RB evaluations required. This occurs because it is no longer demanded that $\mu^{(i)}(k)$ remains within the trust region, allowing the backtracking routine to more quickly return valid steps. These observations underscore that improving TR-RB methods hinges not only on developing better surrogate models but also on finding higher-quality error estimators and more refined conditions to manage the costly re-instantiation of the surrogate models.

Finally, we discuss the characteristics of ML-ROM in an optimization context. We also tested alternative ML methods, including deep neural networks and 2L-VKOGA [52], but did not achieve satisfactory results. This highlights issues that need to be addressed to make machine learning a more reliable foundation for surrogate models. Our experiments reveal that the requirements on the ML algorithm outlined in Section 4.2 are quite restrictive for practical applications. In particular, the constraint that ML methods must train efficiently on limited data prevents the use of more complex models. Combined with the need to guarantee a certain level of accuracy for effective optimization, these constraints limit both the applicability of ML-based optimization and the achievable computational savings.

This issue is exacerbated during optimization, as the parameters for which the ML-ROM is evaluated often lie *outside* of the training data distribution. Consequently, the approximation quality depends more on the hypothesis set and hyperparameters of the model than on the training data itself. This necessitates that the model not only *generalizes* well but also accurately captures the local solution manifold.

However, ensuring adequate generalization requires careful selection of the hypothesis set, balancing model complexity against training time and requirements on the training data. This involves choosing appropriate hyperparameters, kernel functions, and regularization constants, which must be set a priori. Hyperparameter tuning is already challenging, as it requires empirical validation, and becomes even more difficult during optimization, where the training data distribution and required accuracy evolve dynamically. Near the optimum, training data tend to cluster due to frequent backtracking steps, increasing the required accuracy and demanding different kernel parameterizations than those suitable at the start of the optimization. Attempts to adapt hyperparameters dynamically during optimization yielded unpredictable results and did not significantly improve overall performance.

7 Conclusion and Outlook

In this work, we have demonstrated that kernel methods can be effectively applied to optimize quadratic cost functionals constrained by parametrized parabolic PDEs within a trust-region reduced-basis framework, offering a viable approach to reducing computational costs. By learning solutions to the PDE constraints projected onto reduced spaces, the proposed ML-ROM can be certified, while the application of the chain rule enables direct access to the gradient of the cost functional. However, the derived error estimators remain computationally inefficient relative to parameter inference by the ML surrogate. The proposed algorithm addresses this issue by integrating these aspects into a trust-region scheme while circumventing direct reliance on the error estimator. This is achieved by relaxing the TR constraint, ensuring the validity of the surrogates while maintaining computational efficiency. Additionally, the hierarchical model-calling scheme allows the algorithm to dynamically adapt to the current region of interest along the optimization trajectory.

However, as demonstrated in the example of temperature distribution matching, further advancements are necessary to establish ML-based surrogates as a practical choice, particularly for more complex problems. Beyond the need for sharper and

more efficient error estimators and greater robustness to erroneous surrogate models, improvements in the ML models themselves are required. The key challenge is to enable the use of more sophisticated models while maintaining computational feasibility. Future efforts should focus on approaches that incorporate additional information about the PDE constraints alongside training data, such as semi-supervised machine learning methods.

Of particular interest are recent developments in Physics-informed Neural Networks (PINNs) and their variants [32, 53, 54]. These models explicitly integrate PDE constraints into their architecture and, in theory, can produce meaningful global approximations even with limited training data. Incorporating PINNs into the existing framework could therefore be a promising avenue for future research, advancing the integration of ML methods into parametrized parabolic PDE-constrained optimization tasks.

Statements and declarations

Funding. The authors acknowledge funding by the Deutsche Forschungsgemeinschaft (DFG, German Research Foundation) under Germany's Excellence Strategy EXC 2044-390685587, Mathematics Münster: Dynamics–Geometry–Structure.

Competing interests. The authors have no relevant financial or non-financial interests to disclose.

Acknowledgements. Benedikt Klein thanks Hendrik Kleikamp from the University of Münster for the long and fruitful exchange.

References

- [1] Haasdonk, B., Kleikamp, H., Ohlberger, M., Schindler, F., Wenzel, T.: A new certified hierarchical and adaptive RB-ML-ROM surrogate model for parametrized PDEs. *SIAM J. Sci. Comput.* **45**(3), 1039–1065 (2023) <https://doi.org/10.1137/22M1493318>
- [2] Yue, Y., Meerbergen, K.: Accelerating optimization of parametric linear systems by model order reduction. *SIAM Journal on Optimization* **23**(2), 1344–1370 (2013)
- [3] Keil, T., Mechelli, L., Ohlberger, M., Schindler, F., Volkwein, S.: A non-conforming dual approach for adaptive trust-region reduced basis approximation of pde-constrained parameter optimization. *ESAIM: Mathematical Modelling and Numerical Analysis* **55**(3), 1239–1269 (2021) <https://doi.org/10.1051/m2an/2021019>
- [4] Banholzer, S., Keil, T., Ohlberger, M., Mechelli, L., Schindler, F., Volkwein, S.: An adaptive projected Newton non-conforming dual approach for trust-region reduced basis approximation of PDE-constrained parameter optimization. *Pure Appl. Funct. Anal.* **7**(5), 1561–1596 (2022)

- [5] Keil, T., Ohlberger, M.: A relaxed localized trust-region reduced basis approach for optimization of multiscale problems. *ESAIM Math. Model. Numer. Anal.* **58**(1), 79–105 (2024) <https://doi.org/10.1051/m2an/2023089>
- [6] Benner, P., Ohlberger, M., Patera, A., Rozza, G., Urban, K. (eds.): *Model Reduction of Parametrized Systems. MS&A. Modeling, Simulation and Applications*, vol. 17, p. 504. Springer, Cham, Germany (2017). <https://doi.org/10.1007/978-3-319-58786-8> . Selected papers from the 3rd MoRePaS Conference held at the International School for Advanced Studies (SISSA), Trieste, October 13–16, 2015
- [7] Benner, P., Cohen, A., Ohlberger, M., Willcox, K. (eds.): *Model Reduction and Approximation*, p. 412. SIAM, Philadelphia, PA, USA. <https://doi.org/10.1137/1.9781611974829> . Theory and algorithms
- [8] Haasdonk, B., Ohlberger, M.: Reduced basis method for finite volume approximations of parametrized linear evolution equations. *Mathematical Modelling and Numerical Analysis* **42**(2), 277–302 (2008) <https://doi.org/10.1051/m2an:2008001>
- [9] Haasdonk, B.: Convergence rates of the POD-greedy method. *ESAIM Math. Model. Numer. Anal.* **47**(3), 859–873 (2013) <https://doi.org/10.1051/m2an/2012045>
- [10] Himpe, C., Leibner, T., Rave, S.: Hierarchical approximate proper orthogonal decomposition. *SIAM Journal on Scientific Computing* **40**(5), 3267–3292 (2018)
- [11] Kammann, E., Tröltzsch, F., Volkwein, S.: A posteriori error estimation for semilinear parabolic optimal control problems with application to model reduction by POD. *ESAIM: M2AN* **47**(2), 555–581 (2013) <https://doi.org/10.1051/m2an/2012037>
- [12] Grepl, M.A., Kärcher, M.: Reduced basis a posteriori error bounds for parametrized linear-quadratic elliptic optimal control problems. *C. R. Math. Acad. Sci. Paris* **349**(15-16), 873–877 (2011) <https://doi.org/10.1016/j.crma.2011.07.010>
- [13] Negri, F., Rozza, G., Manzoni, A., Quateroni, A.: Reduced basis method for parametrized elliptic optimal control problems. *SIAM J. Sci. Comput.* **35**(5), 2316–2340 (2013) <https://doi.org/10.1137/120894737>
- [14] Hinze, M.: Model order reduction for optimal control problems. In: *Model Order Reduction and Applications. Lecture Notes in Math.*, vol. 2328, pp. 125–199. Springer, Cham, Germany ([2023] ©2023). https://doi.org/10.1007/978-3-031-29563-8_3
- [15] Zahr, M.J., Farhat, C.: Progressive construction of a parametric reduced-order model for PDE-constrained optimization. *Internat. J. Numer. Methods Engrg.*

102(5), 1111–1135 (2015) <https://doi.org/10.1002/nme.4770>

- [16] Garmatter, D., Haasdonk, B., Harrach, B.: A reduced basis Landweber method for nonlinear inverse problems. *Inverse Problems* **32**(3), 035001–21 (2016) <https://doi.org/10.1088/0266-5611/32/3/035001>
- [17] Ohlberger, M., Schaefer, M., Schindler, F.: Localized model reduction in PDE constrained optimization. In: *Shape Optimization, Homogenization and Optimal Control. Internat. Ser. Numer. Math.*, vol. 169, pp. 143–163. Birkhäuser/Springer, Cham, Germany (2018)
- [18] Rogg, S., Trenz, S., Volkwein, S.: Trust-region POD using a-posteriori error estimation for semilinear parabolic optimal control problems. *Konstanzer Schriften in Mathematik No. 359* (2017)
- [19] Qian, E., Grepl, M., Veroy, K., Willcox, K.: A certified trust region reduced basis approach to PDE-constrained optimization. *SIAM Journal on Scientific Computing* **39**(5), 434–460 (2017)
- [20] Wen, T., Zahr, M.J.: A globally convergent method to accelerate large-scale optimization using on-the-fly model hyperreduction: application to shape optimization. *J. Comput. Phys.* **484**, 112082–33 (2023) <https://doi.org/10.1016/j.jcp.2023.112082>
- [21] Hesthaven, J.S., Ubbiali, S.: Non-intrusive reduced order modeling of nonlinear problems using neural networks. *Journal of Computational Physics* **363**, 55–78 (2018)
- [22] Kutyniok, G., Petersen, P., Raslan, M., Schneider, R.: A theoretical analysis of deep neural networks and parametric PDEs. *Constr. Approx.* **55**(1), 73–125 (2022) <https://doi.org/10.1007/s00365-021-09551-4>
- [23] Fresca, S., Manzoni, A.: POD-DL-ROM: Enhancing deep learning-based reduced order models for nonlinear parametrized pdes by proper orthogonal decomposition. *Computer Methods in Applied Mechanics and Engineering* **388**, 114181 (2022)
- [24] Conti, P., Guo, M., Manzoni, A., Hesthaven, J.S.: Multi-fidelity surrogate modeling using long short-term memory networks. *Comput. Methods Appl. Mech. Engrg.* **404**, 115811–22 (2023) <https://doi.org/10.1016/j.cma.2022.115811>
- [25] Brivio, S., Fresca, S., Franco, N.R., Manzoni, A.: Error estimates for POD-DL-ROMs: a deep learning framework for reduced order modeling of nonlinear parametrized PDEs enhanced by proper orthogonal decomposition. *Adv. Comput. Math.* **50**(3), 33–46 (2024) <https://doi.org/10.1007/s10444-024-10110-1>

- [26] Gavrilenko, P., Haasdonk, B., Iliev, O., Ohlberger, M., Schindler, F., Toktaliev, P., Wenzel, T., Youssef, M.: A full order, reduced order and machine learning model pipeline for efficient prediction of reactive flows. In: Large-scale Scientific Computing. Lecture Notes in Comput. Sci., vol. 13127, pp. 378–386. Springer, Berlin, Germany ([2022] ©2022). https://doi.org/10.1007/978-3-030-97549-4_43
- [27] Wenzel, T., Haasdonk, B., Kleikamp, H., Ohlberger, M., Schindler, F.: Application of deep kernel models for certified and adaptive RB-ML-ROM surrogate modeling. In: Large-scale Scientific Computations. Lecture Notes in Comput. Sci., vol. 13952, pp. 117–125. Springer, Cham ([2024] ©2024). https://doi.org/10.1007/978-3-031-56208-2_11
- [28] Lye, K.O., Mishra, S., Ray, D., Chandrashekar, P.: Iterative surrogate model optimization (ismo): An active learning algorithm for pde constrained optimization with deep neural networks. *Computer Methods in Applied Mechanics and Engineering* **374**, 113575 (2021)
- [29] Keil, T., Kleikamp, H., Lorentzen, R.J., Oguntola, M.B., Ohlberger, M.: Adaptive machine learning-based surrogate modeling to accelerate PDE-constrained optimization in enhanced oil recovery. *Advances in Computational Mathematics* **48**(6), 73 (2022)
- [30] Xu, K., Darve, E.: Physics Constrained Learning for Data-driven Inverse Modeling from Sparse Observations (2020). <https://arxiv.org/abs/2002.10521>
- [31] Kleikamp, H., Lazar, M., Molinari, C.: Be greedy and learn: efficient and certified algorithms for parametrized optimal control problems. *ESAIM Math. Model. Numer. Anal.* **59**(1), 291–330 (2025) <https://doi.org/10.1051/m2an/2024074>
- [32] Raissi, M., Perdikaris, P., Karniadakis, G.E.: Physics-informed neural networks: A deep learning framework for solving forward and inverse problems involving nonlinear partial differential equations. *Journal of Computational physics* **378**, 686–707 (2019)
- [33] E, W., Yu, B.: The deep Ritz method: a deep learning-based numerical algorithm for solving variational problems. *Commun. Math. Stat.* **6**(1), 1–12 (2018) <https://doi.org/10.1007/s40304-018-0127-z>
- [34] Milk, R., Rave, S., Schindler, F.: pyMOR – generic algorithms and interfaces for model order reduction. *SIAM Journal on Scientific Computing* **38**(5), 194–216 (2016) <https://doi.org/10.1137/15m1026614>
- [35] Hinze, M., Pinnau, R., Ulbrich, M., Ulbrich, S.: *Optimization with PDE Constraints* vol. 23. Springer, Berlin, Germany (2009)
- [36] Quarteroni, A., Manzoni, A., Negri, F.: *Reduced Basis Methods for Partial*

Differential Equations: an Introduction vol. 92. Springer, Berlin, Germany (2015)

- [37] Grepl, M.A., Patera, A.T.: A posteriori error bounds for reduced-basis approximations of parametrized parabolic partial differential equations. *ESAIM: Mathematical Modelling and Numerical Analysis* **39**(1), 157–181 (2005)
- [38] Haasdonk, B.: Chapter 2: Reduced Basis Methods for Parametrized PDEs - A Tutorial Introduction for Stationary and Instationary Problems, pp. 65–136. <https://doi.org/10.1137/1.9781611974829.ch2>
- [39] Buhr, A., Engwer, C., Ohlberger, M., Rave, S.: A numerically stable a posteriori error estimator for reduced basis approximations of elliptic equations (2014) [arXiv:1407.8005](https://arxiv.org/abs/1407.8005) [math.NA]
- [40] Kutyniok, G., Petersen, P., Raslan, M., Schneider, R.: A theoretical analysis of deep neural networks and parametric pdes (2020) [arXiv:1904.00377](https://arxiv.org/abs/1904.00377) [math.NA]
- [41] Goodfellow, I.J., Bengio, Y., Courville, A.: *Deep Learning*. MIT Press, Cambridge, MA, USA (2016)
- [42] LeCun, Y., Bengio, Y., Hinton, G.: Deep learning. *nature* **521**(7553), 436–444 (2015)
- [43] Berner, J., Grohs, P., Kutyniok, G., Petersen, P.: The modern mathematics of deep learning. *arXiv preprint arXiv:2105.04026*, 86–114 (2021)
- [44] Kutyniok, G.: The mathematics of artificial intelligence. *arXiv preprint arXiv:2203.08890* (2022)
- [45] Kleikamp, H.: Application of an adaptive model hierarchy to parametrized optimal control problems. *arXiv preprint arXiv:2402.10708* (2024)
- [46] Kleikamp, H., Ohlberger, M.: Adaptive Model Hierarchies for Multi-Query Scenarios (2024). <https://arxiv.org/abs/2411.17252>
- [47] Kelley, C.T.: *Iterative Methods for Optimization*. SIAM, Philadelphia, PA, USA (1999)
- [48] Rasmussen, C.E., Williams, C.K.: *Gaussian Processes for Machine Learning*, Ser. Adaptive Computation and Machine Learning vol. 38, pp. 715–719 (2006)
- [49] Schaback, R., Wendland, H.: Kernel techniques: from machine learning to meshless methods. *Acta numerica* **15**, 543–639 (2006)
- [50] Santin, G., Haasdonk, B.: Kernel methods for surrogate modeling. *Model Order Reduction* **1**, 311–354 (2019)
- [51] Klein, B., Ohlberger, M.: *Software for Multi-fidelity Learning of Reduced*

Order Models for Parabolic PDE Constrained Optimization. Zenodo (2025).
<https://doi.org/10.5281/zenodo.15063806>

- [52] Wenzel, T., Marchetti, F., Perracchione, E.: Data-driven kernel designs for optimized greedy schemes: A machine learning perspective (2023) [arXiv:2301.08047](https://arxiv.org/abs/2301.08047) [math.NA]
- [53] Yu, B., *et al.*: The deep ritz method: a deep learning-based numerical algorithm for solving variational problems. *Communications in Mathematics and Statistics* **6**(1), 1–12 (2018)
- [54] Tanyu, D.N., Ning, J., Freudenberg, T., Heilenkötter, N., Rademacher, A., Iben, U., Maass, P.: Deep learning methods for partial differential equations and related parameter identification problems. *Inverse Problems* **39**(10), 103001 (2023)

Appendix A ML a posteriori error estimator

A.1 Proof of Lemma 4.2

Proof The high-fidelity solution map $\mu \mapsto u_h(\mu) \in Q_{\Delta t}^{\text{PF}}(0, T; V_h)$ is Fréchet differentiable. For all $k \in \mathbb{K}$ and $i \in \{1, \dots, P\}$. $d_{\mu_i} u_h^k(\mu)$ can be obtained as the unique solution of

$$d_{\mu_i} r_{\text{pr}}^k(u_h^k, v; \mu) = a(d_{\mu_i} u_h^k(\mu), v; \mu) + \frac{1}{\Delta t} (d_{\mu_i} u_h^k(\mu) - d_{\mu_i} u_h^{k-1}(\mu), v)_{L^2(\Omega)}, \quad (\text{A1})$$

for all $v \in V_h$ with initial condition $d_{\mu_i} u_h^0(\mu) = 0$, cf. [35, Section 1.6.1]. Adding (17) and (A1) gives

$$a(d_{\mu_i} e^k, v; \mu) + \frac{1}{\Delta t} (d_{\mu_i} e^k(\mu) - d_{\mu_i} e^{k-1}(\mu), v)_{L^2(\Omega)} = \mathcal{R}_{\text{ML}}^k(v; \mu) + d_{\mu_i} r_{\text{pr}}^k(e^k(\mu), v; \mu),$$

where $e^k(\mu) := u_h^k(\mu) - u_{\text{ML}}^k(\mu)$ and $d_{\mu_i} e^k(\mu) := d_{\mu_i} u_h^k(\mu) - d_{\mu_i} u_{\text{ML}}^k(\mu)$. Setting $v := d_{\mu_i} e^k(\mu)$ and using

$$d_{\mu_i} r_{\text{pr}}^k(e^k(\mu), v; \mu) = d_{\mu_i} a(-e^k(\mu), v; \mu) \leq \gamma_{a_{\mu_i}}(\mu) \|e^k(\mu)\|_{V_h} \|v\|_{V_h},$$

for all $v \in V_h$ gives

$$\begin{aligned} & (d_{\mu_i} e^k(\mu), d_{\mu_i} e^k(\mu))_{L^2(\Omega)} + \Delta t a(d_{\mu_i} e^k, d_{\mu_i} e^k(\mu); \mu) \\ & \leq (d_{\mu_i} e^{k-1}(\mu), d_{\mu_i} e^k(\mu))_{L^2(\Omega)} + \Delta t \left(\|\mathcal{R}_{\text{ML}}^k(\cdot; \mu)\|_{V_h'} + \gamma_{a_{\mu_i}}(\mu) \|e^k(\mu)\|_{V_h} \right) \|d_{\mu_i} e^k(\mu)\|_{V_h} \end{aligned}$$

Analogue to the proof of Proposition 4.1 in [37] remark firstly

$$\begin{aligned} & (d_{\mu_i} e^{k-1}(\mu), d_{\mu_i} e^k(\mu))_{L^2(\Omega)} \\ & \leq \frac{1}{2} \left((d_{\mu_i} e^{k-1}(\mu), d_{\mu_i} e^{k-1}(\mu))_{L^2(\Omega)} + (d_{\mu_i} e^k(\mu), d_{\mu_i} e^k(\mu))_{L^2(\Omega)} \right) \end{aligned}$$

and secondly

$$\begin{aligned} & \left(\|\mathcal{R}_{\text{ML}}^k(\cdot; \mu)\|_{V_h'} + \gamma_{a_{\mu_i}}(\mu) \|e^k(\mu)\|_{V_h} \right) \|d_{\mu_i} e^k(\mu)\|_{V_h} \\ & \leq \frac{1}{2\alpha_{\text{LB}}(\mu)} \left(\|\mathcal{R}_{\text{ML}}^k(\cdot; \mu)\|_{V_h'} + \gamma_{a_{\mu_i}}(\mu) \|e^k(\mu)\|_{V_h} \right)^2 + \frac{1}{2} a(d_{\mu_i} e^k(\mu), d_{\mu_i} e^k(\mu); \mu), \end{aligned}$$

resulting in

$$\begin{aligned} & (d_{\mu_i} e^k(\mu), d_{\mu_i} e^k(\mu))_{L^2(\Omega)} - (d_{\mu_i} e^{k-1}(\mu), d_{\mu_i} e^{k-1}(\mu))_{L^2(\Omega)} + \Delta t a(d_{\mu_i} e^k(\mu), d_{\mu_i} e^k(\mu); \mu) \\ & \leq \frac{\Delta t}{\alpha_{\text{LB}}(\mu)} \left(\|\mathcal{R}_{\text{ML}}^k(\cdot; \mu)\|_{V_h'}^2 + \gamma_{a_{\mu_i}}^2(\mu) \|e^k(\mu)\|_{V_h}^2 + 2\gamma_{a_{\mu_i}}(\mu) \|\mathcal{R}_{\text{ML}}^k(\cdot; \mu)\|_{V_h'} \|e^k(\mu)\|_{V_h} \right) \end{aligned}$$

Taking the sum over $k \in \mathbb{K}$ and using $d_{\mu_i} e^0(\mu) = 0$ results in

$$\begin{aligned} \alpha_{\text{LB}}(\mu) \mathcal{S}^2(d_{\mu_i} e(\mu)) & \leq \alpha_{\text{LB}}^{-1}(\mu) \mathcal{T}^2(\mathcal{R}_{\text{ML}}(\cdot; \mu)) \\ & \quad + \alpha_{\text{LB}}^{-1}(\mu) \gamma_{a_{\mu_i}}^2(\mu) \mathcal{S}^2(e(\mu)) + 2\alpha_{\text{LB}}^{-1}(\mu) \gamma_{a_{\mu_i}}(\mu) \mathcal{T}(\mathcal{R}_{\text{ML}}(\cdot; \mu)) \mathcal{S}(e(\mu)) \end{aligned}$$

with $e(\mu) := u_h(\mu) - u_{\text{ML}}(\mu)$. This proves the claim. \square

A.2 Proof of Theorem 4.3

Proof For (18) consider the first part of the proof to Theorem 9 in [19], obtaining

$$e^{\mathcal{J}}(\mu) := \mathcal{J}_h(\mu) - \mathcal{J}_{\text{ML}}(\mu) = \Delta t \sum_{k=1}^K \left[2d(u_{\text{ML}}^k(\mu), e^k(\mu)) + l^k(e^k(\mu)) + d(e^k(\mu), e^k(\mu)) \right]$$

for $e^k(\mu) := u_h^k(\mu) - u_{\text{ML}}^k(\mu)$. Substituting $l^k(e^k(\mu)) = d(g_{\text{ref}}^k, e^k(\mu))$ results in

$$|e^{\mathcal{J}}(\mu)| \leq \gamma_d \Delta t \sum_{k=1}^K \left[2\|u_{\text{ML}}^k(\mu)\|_{V_h} \|e^k(\mu)\|_{V_h} + \|g_{\text{ref}}^k\|_{V_h} \|e^k(\mu)\|_{V_h} + \|e^k(\mu)\|_{V_h}^2 \right].$$

Applying Cauchy-Schwarz inequality and using (16) proves the claim. To prove the second inequality (19) denote

$$\begin{aligned} e^{d_{\mu_i} \mathcal{J}}(\mu) & := d_{\mu_i} \mathcal{J}_h(\mu) - d_{\mu_i} \mathcal{J}_{\text{ML}}(\mu) \\ & = \Delta t \sum_{k=1}^K \left[\underbrace{2d(u_h^k(\mu), d_{\mu_i} u_h^k(\mu)) - 2d(u_{\text{ML}}^k(\mu), d_{\mu_i} u_{\text{ML}}^k(\mu))}_{=: (*)} + d(g_{\text{ref}}^k, d_{\mu_i} e^k(\mu)) \right]. \end{aligned}$$

Adding and subtracting

$$\Delta t \sum_{k=1}^K \left[2d(u_h^k(\mu), d_{\mu_i} u_{\text{ML}}^k(\mu)) + 2d(u_{\text{ML}}^k(\mu), d_{\mu_i} e^k(\mu)) \right]$$

to (*) gives

$$\begin{aligned} (*) & = \Delta t \sum_{k=1}^K \left[2d(u_h^k(\mu), d_{\mu_i} e^k(\mu)) + 2d(e^k(\mu), d_{\mu_i} u_{\text{ML}}^k(\mu)) \right] \\ & \quad + \Delta t \sum_{k=1}^K \left[2d(u_{\text{ML}}^k(\mu), d_{\mu_i} e^k(\mu)) - 2d(u_{\text{ML}}^k(\mu), d_{\mu_i} e^k(\mu)) \right] \\ & = \Delta t \sum_{k=1}^K \left[2d(e^k(\mu), d_{\mu_i} e^k(\mu)) + 2d(e^k(\mu), d_{\mu_i} u_{\text{ML}}^k(\mu)) + 2d(u_{\text{ML}}^k(\mu), d_{\mu_i} e^k(\mu)) \right]. \end{aligned}$$

Resulting in

$$\begin{aligned} |e^{d_{\mu_i} \mathcal{J}}(\mu)| & \leq \gamma_d \Delta t \sum_{k=1}^K \left[2\|e^k(\mu)\|_{V_h} \|d_{\mu_i} e^k(\mu)\|_{V_h} + 2\|e^k(\mu)\|_{V_h} \|d_{\mu_i} u_{\text{ML}}^k(\mu)\|_{V_h} \right] \\ & \quad + \gamma_d \Delta t \sum_{k=1}^K \left[2\|u_{\text{ML}}^k(\mu)\|_{V_h} \|d_{\mu_i} e^k(\mu)\|_{V_h} + \|g_{\text{ref}}^k\|_{V_h} \|d_{\mu_i} e^k(\mu)\|_{V_h} \right]. \end{aligned}$$

The claim follows with Lemma 4.2. \square